Hindawi
Advances in Civil Engineering
Volume 2024, Article ID 1784088, 22 pages
https://doi.org/10.1155/2024/1784088

Research Article

Comparative Analysis of Shear Strength Prediction Models for Reinforced Concrete Slab–Column Connections

Sarmed Wahab,[1] Nasim Shakouri Mahmoudabadi,[2] Sarmad Waqas,[3] Nouman Herl,[4] Muhammad Iqbal,[5] Khurshid Alam,[6] and Afaq Ahmad [1,2]

[1]*Civil Engineering Department, University of Engineering and Technology, Taxila, Rawalpindi, Pakistan*
[2]*Department of Civil Engineering, The University of Memphis, Memphis, TN 38152, USA*
[3]*Osmani and Company Pvt. Ltd., Karachi, Pakistan*
[4]*Federal Board of Intermediate and Secondary Education, Islamabad, Pakistan*
[5]*Department of Mechanical Engineering, CECOS University of IT and Emerging Sciences, Hayatabad, Peshawar 25000, Pakistan*
[6]*Department of Mechanical and Industrial Engineering, College of Engineering, Sultan Qaboos University, Muscat, Oman*

Correspondence should be addressed to Afaq Ahmad; afaq.ahmad@uettaxila.edu.pk

Received 4 December 2023; Revised 21 January 2024; Accepted 2 February 2024; Published 6 March 2024

Academic Editor: Gang Mei

This research focuses on a comprehensive comparative analysis of shear strength prediction in slab–column connections, integrating machine learning, design codes, and finite element analysis (FEA). The existing empirical models lack the influencing parameters that decrease their prediction accuracy. In this paper, current design codes of American Concrete Institute 318-19 (ACI 318-19) and Eurocode 2 (EC2), as well as innovative approaches like the compressive force path method and machine learning models are employed to predict the punching shear strength using a comprehensive database of 610 samples. The database consists of seven key parameters including slab depth (d_s), column dimension (c_s), shear span ratio (a_v/d), yield strength of longitudinal steel (f_y), longitudinal reinforcement ratio (ρ_l), ultimate load-carrying capacity (V_u), and concrete compressive strength (f_c). Compared with the design codes and other machine learning models, the particle swarm optimization-based feedforward neural network (PSOFNN) performed the best predictions. PSOFNN predicted the punching shear of flat slab with maximum accuracy with R^2 value of 99.37% and least MSE and MAE values of 0.0275% and 1.214%, respectively. The findings of the study are validated through FEA of slabs to confirm experimental results and machine learning predictions that showed excellent agreement with PSOFNN predictions. The research also provides insight into the application of metaheuristic models along with ANN, revealing that not all metaheuristic models can outperform ANN as usually perceived. The study also highlights superior predictive capabilities of EC2 over ACI 318-19 for punching shear values.

1. Introduction

Flat slabs are favored in the construction of reinforced concrete (RC) structures due to their economic and efficient nature [1, 2]. They are positioned directly over columns without beams, which facilitates a direct transfer of load from the slab to the columns. The absence of beams offers several advantages, including reduced building height, easy integration of vertical shafts, layout flexibility, simplified reinforcement placement, faster construction, and form simplification [2–4]. The design of a flat slab is mainly controlled by punching shear that exists at the vicinity of the slab–column connection due to high shear stresses. The punching leads to a complete loss of shear capacity at the slab–column connection, leading to brittle failure of the slab–column connection [5], as shown in Figure 1. Due to this failure, the loads are redistributed to the adjacent structural elements leading to a progressive failure. Determination of punching shear failure of the flat slab is a complex task due to numerous factors and may be caused due to large column loads, insufficient concrete strength [6], inadequate slab thickness [7], insufficient shear reinforcement [8], small column heads, and poor construction

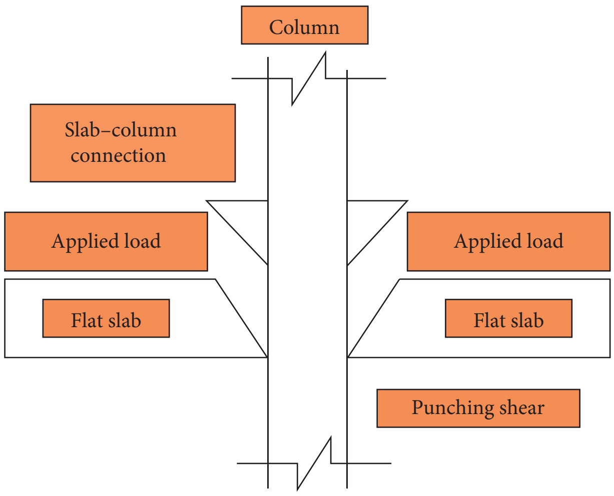

Figure 1: Punching shear failure at slab–column connection.

quality. Numerous experimental studies have been conducted to assess the performance of flat slabs. Some of the empirical models have been used in the design codes [9]. The existing empirical models [10–15] were developed from the experimental values using the regression analysis. Therefore, their performance is dependent on the database used to determine the punching shear strength. The results of these empirical models have shown variation in their results, resulting in under or overprediction of punching shear values [16].

Despite having various methodologies to determine the punching shear strength of flat slabs, these approaches only work under specific frameworks. Such difficulties in the empirical methods can be avoided by using machine learning (ML) algorithms. Researchers have used artificial neural networks (ANNs) in the prediction of load carrying capacity of RC members [17], the elastic behavior of normal and high-strength concrete [18], the structural behavior of slabs [16], the ultimate strength of beams [19], the rutting performance of asphalt mixtures containing steel slag aggregates [20], and prediction of the behavior of shear connectors in concrete [21]. These machine learning models have demonstrated their effectiveness in determining the performance of various structural members. ANN has been used to predict the load-carrying capacity of structural members like the strength prediction of RC beams [22, 23] and columns [24–26]. However, ANN suffers from local optima problems resulting in incomplete exploration of the dataset leading to wrong predictions. The performance of ANN can be optimized using metaheuristic algorithms. There are numerous ways in which ANN can be optimized including optimizing the architecture of the neural network, weight optimization, activation nodes, and parameters involved in the network [27]. The major advantages of metaheuristic algorithms over ANN are their ability to provide the optimum value of weights of the network after performing optimization and their ability to elude being trapped in local minima and multivariability [28].

A hybrid model of adaptive neuro-fuzzy inference systems combined with a genetic algorithm and particle swarm optimization has been used to predict the shear strength of RC beams [29]. The hybrid model predicted shear strength with greater accuracy compared to standalone models. In another study, an informational Bat ANN was applied to predict the punching shear strength of RC flat slabs without shear reinforcement [30]. The research investigated 30 distinct topologies of the model to identify the best possible prediction model with minimized errors and the highest R^2 values. Nolan Concha et al. [31] implemented a hybrid neural network of particle swarm optimization to predict the shear strength of steel fiber RC deep beams [32, 33]. The hybrid model predicted the strength of a steel fiber-RC deep beam with a correlation coefficient of 0.997. The high accuracy of these hybrid prediction models provides a suitable tool to predict structural performance. Sandeep et al. [34] used machine learning to predict the shear strength of RC beams. Researchers used atom search optimization (ASO) algorithm combined with neural network to predict the shear strength of beams. These results were then compared with the prediction results of various hybrid and standalone models including ANN, genetic algorithm, particle swarm optimized neural network, and support vector machines.

The present study is aimed at the prediction of punching shear strength at the slab–column connection in flat slabs using a comprehensive dataset of flat slabs and to provide a comparison of the performance of current design codes (CDCs) with the prediction models. This study aims to predict the punching shear of a flat slab by using three different ML models, one of which is feedforward neural network (FNN) the particle swarm optimization-based FNN (PSOFNN), and Bat algorithm-based FNN (BATFNN). A comprehensive dataset consisting of 610 samples is collected from previously published research. The parameters involved in the dataset are column parameter (b), slab depth (d_s), column dimension (c_s), longitudinal steel yield strength (f_y), percentage of longitudinal steel ratio (ρ_l), ultimate load carrying capacity (V_u), and concrete compressive strength (f_c). These data are converted to seven different subsets of concrete slab (SCS) using the parameters from the original database to evaluate the influence of different parameters on the punching shear strength of a flat slab. The working of the prediction models is evaluated using mean square error, mean absolute error (MAE), and R-value. The predicted punching shear values are compared with calculated values from CDCs and compressive force path (CFP) that revealed that design codes result in punching shear values less than the actual experimental values [35–37]. From the prediction results performed in this study, it has been observed that PSOFNN provided more accurate predictions for punching shear strength than ANN and BATFNN. To validate the prediction results of PSOFNN, finite element analysis (FEM) is used, which provided good correspondence with the predicted results from PSOFNN and ANN.

2. Empirical Models

This research adopts the innovative CFP method, as introduced by Kotsovos [38], to enhance the punching shear strength of flat slabs. The CFP method strategically designs structural elements to ensure the efficient transmission of compressive forces from the slab to the columns, thereby reducing tensile stresses at the slab–column interface and enhancing punching shear strength. Key design considerations within the CFP method encompass the geometry and dimensions of the column, the size and spacing of reinforcement, and the arrangement of reinforcement around the column. The method aims to establish a force path for compressive forces that minimizes tensile stresses at the slab–column interface. A pivotal feature is the incorporation of a wider column head, facilitating a more efficient distribution of compressive forces from the slab to the column and mitigating tensile stresses. Effective reinforcement design is paramount in improving the punching shear strength within the CFP method. This involves arranging reinforcement around the column in a circular or square pattern, with suitable spacing and size. Placing the reinforcement close to the slab surface maximizes its effectiveness in reducing tensile stresses. Additionally, the use of shear studs or connectors enhances the bond between reinforcement and concrete, facilitating the more efficient transfer of compressive forces and overall slab strength. The CFP method stands out for its simplicity and adaptability across various structural systems. Particularly beneficial for structures with large flat slabs and heavy column loads, it addresses the critical design consideration of punching shear failure in such scenarios.

The CDCs, such as American Concrete Institute 318-19 (ACI 318-19) and Eurocode 2 (EC2), were developed with a focus on providing economical and safer structural designs through a limit-state design approach based on theoretical frameworks. However, these design methods, effective for steel structures, prove less suited for concrete structures under ultimate load conditions, as highlighted by Kotsovos [38]. The unreliability of CDCs has been observed in structural elements like columns, beams, beam–column joints, and walls, where experimental results often deviate significantly from CDC predictions. In contrast to CDCs, the CFP method introduces significant improvements. The first enhancement involves determining the areas within structural members where applied loads are transferred from their point of application to the supports. The second improvement focuses on strengthening these areas to enhance structural ductility and load-carrying capacity, addressing the limitations of CDCs. This method, as outlined by Kotsovos [38], successfully meets all code performance requirements at both structural and material levels. The CFP method thus presents a promising alternative, ensuring more accurate predictions and aligning with the principles of safer and more economical limit state design.

Truss analogy models in mechanics, as applied to the ultimate limit response (ULR) of concrete slab, provide a theoretical framework for load transfer [17]. In this method, force transmission is conceptualized in a triangular fashion. It is notable that the equations employed by ACI and EC2 are empirical [39, 40], leading to data fitting, and are prone to structural failures, including collapse [41]. The nature of analysis formulas in CDCs introduces a significant

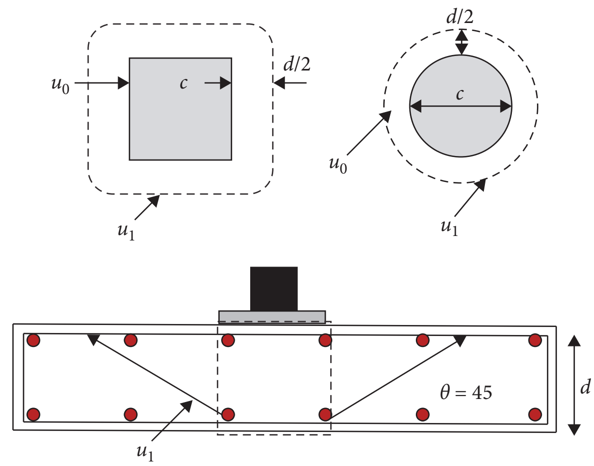

Figure 2: ACI-based boundary for SCS.

divergence between values calculated using CDCs and experimental values. Despite this discrepancy, CDCs are frequently utilized by engineering professionals due to their ease of application in testing flat slab–column connections at the ULR. Several parameters, including slab depth (d_s), column dimension (c_s), shear span ratio (a_v/d), longitudinal reinforcement yield strength (f_y), longitudinal reinforcement ratio (ρ_l), ultimate load carrying capacity (V_u), and compressive strength of concrete (f_c), are considered by CDCs in determining the punching failure of slabs. The SCS response is predicted using Equation (1) for ACI 318-19 based boundary conditions, as shown in Figure 2:

$$V_{rc} = \frac{1}{3} \times \lambda_s \times u_{2s} \times d_s \times \sqrt{f_c'}, \tag{1}$$

and

$$\lambda_s = \sqrt{\frac{2}{1 + 0.004d}} \leq 1, \tag{2}$$

$$u_{2s} = 4(c + d). \tag{3}$$

The following equation is used in EC2 for the prediction of slab response, as shown in Figure 3:

$$V_{rc} = 0.18 \times u_1 \times d \times \left(1 + \sqrt{\frac{200}{d}}\right) \times \sqrt[3]{100 \times f_c' \times \rho_s}, \tag{4}$$

and

$$\rho_s = \sqrt{\rho_x \rho_y}, \text{and } \rho_x, \rho_y, \tag{5}$$

where ρ_x and ρ_y are x and y direction reinforcement ratios of the slab, respectively. CDC is based on the truss analogy approach; however, CFP is based on the structural response

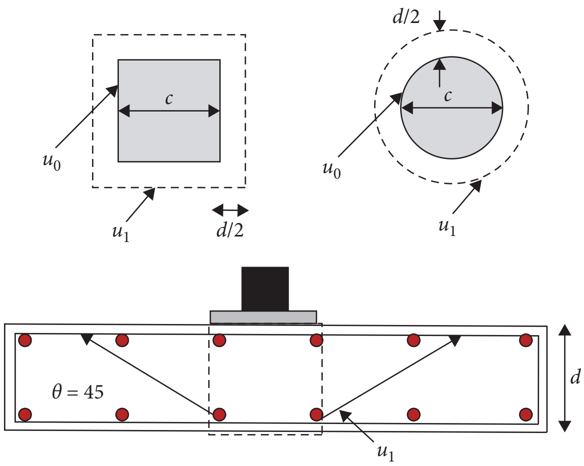

FIGURE 3: EC2-based boundary for SCS.

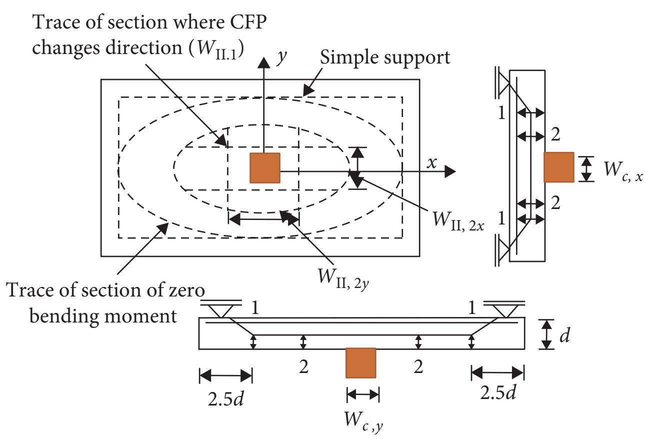

FIGURE 4: CFP-based punching failure assumption of SCS.

of an arch-like frame at ULR as represented in Figure 4. The equations are as follows:

$$W_{II,2} = W_C + (2\lambda_c d), \tag{6}$$

$$\lambda_c = 2 - \left[\frac{100\rho_l f_y}{500}\right][1 + 0.01(f_c - 60)] \, . \tag{7}$$

3. Soft Computing Methods

Soft computing methods such as machine learning are an alternative to the analytical approach. This study uses three such techniques based on machine learning including feed FNN, particle swarm optimization-based FNN (PSOFNN), and bat algorithm-based FNN (BATFNN). The author's previous work [42] included only ANN as a soft computing approach for determining the punching shear strength of flat slabs and since then the ACI code has also been revised. This study includes two more techniques of PSOFNN and BATFNN and an updated version of ACI 318-19 for calculating the shear strength of flat slabs.

3.1. Artificial Neural Network (ANN). ANN is a powerful artificial intelligence tool developed to mimic the workings of the human brain [43]. Neural networks have several unique features that enable them to be implemented in various fields of study. They can be used in data processing, image processing, prediction, and classification [19]. The ANN architecture consists of neurons and layers, where the layers are divided into input, hidden, and output layers [20] that contain neurons. The input layer receives the data from the model, these data are transferred to the hidden layers. The neurons are linked together through weights which are multiplied by the neurons generated values which are then added with the bias. These weights are randomly initialized, and they are updated on each iteration to lessen the difference between the input and the predicted values for the later iterations. Multilayer feedforward ANN (MLFNN) consists of an interconnected perceptron in which data flows from the input to the output layer. The number of layers in the network is the number of layers of the perceptron. A simple neural network consists of a single input and output layer, this is called a one-layer FNN. Adding intermediate hidden layers to the network increases the complexity of the network. Hidden layers perform the computation on the data using activation functions that enable the output layer of the ANN to perform predictions [18]. The inputs and predictions are evaluated by the neural network for errors and these errors are propagated from the output node to the input node. The neural network keeps on reducing errors based on the provided conditions during the initialization of the network training. These conditions can be the number of iterations, the performance goal of the network, and maximum validation failures.

3.2. Particle Swarm Optimization. Particle swarm optimization is an intelligent optimization algorithm belonging to a class of nature-inspired algorithms called metaheuristics. It is based on the social behavior of animals like birds and fish. Fish and birds modify their movements to seek food and avoid predators [44]. It is applied in various fields of science and engineering. PSO uses several particles to make a swarm that searches for the best solution in the search space. In PSO, every particle has three main parameters that are the velocity of the particle, particle position, and the previous best position of the particle [45, 46]. With each successive iteration of the PSO, the particles try to converge to the best position $\vec{x}_i(t+1)$ by adjusting their position $\vec{x}_i(t)$ and velocity $\vec{v}_i(t)$ by keeping track of their experience, as shown in Figure 5.

The particle in the swarm having the best personal value for fitness is taken as the global best. A summary of working of the PSO is creating a swarm population consisting of particles having a velocity and position, every particle has a memory of its best position that is termed as personal best and there exists a common best experience among members of the swarm known as global best. Every member updates their position based on their personal best and global best

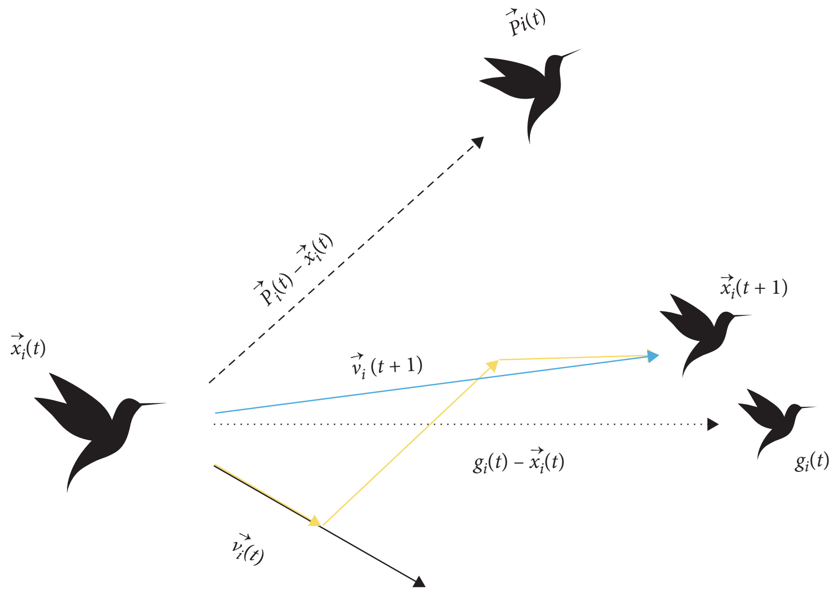

Figure 5: Adjustment of velocity and position in PSO algorithm.

which helps them to converge [47]. The working of the PSO algorithm is represented in a flowchart in Figure 6. In this study, the hyperparameters of the PSO are optimized using a grid search to identify the combination that results in optimal model performance. The hyperparameters of the PSO algorithm are swarm size, inertia weight, cognitive weight, social weight, maximum iterations performed for convergence, and velocity limits. The size of the swarm determines the number of particles employed for optimization. The potential of discovering a global optimum increases as the size of the swarm does, but it does become computationally expensive. The best value of the swarm size is based on the problem being solved as it depends on the complexity of the problem, its dimensionality, size of the search space thus it may vary.

The inertia weight, cognitive weight, and social weight are what govern the algorithm's behavior when it comes to exploration and exploitation. The influence of the particle's former velocity on its current movement is determined by the inertia weight. The inclination of the particle to travel toward its optimal position is controlled by the cognitive weight. A higher value indicates that the particle's previous best position will have a bigger influence on the current movement. The tendency of the particle to move toward the swarm's optimal position on a global scale is controlled by the social weight. The inclination of the particle to go in the same direction as it did in the previous iteration will rise as inertia weight increases. Increasing cognitive weight can make the algorithm more aggressive in its exploration of the search space by increasing the tendency of the particle to advance toward its own personal best position. Increasing the value of all these three weights can make the algorithm converge faster but also increase the chances of getting stuck in a local optimum.

3.3. BAT Algorithm. The bat algorithm (BA) was proposed by Yang [48] to imitate the echolocation behavior of bats [49]. The echolocation ability of bats enables them to not only search for prey but also differentiate between prey and obstacles in the path. Bats produce loud sound pulses and when these pulses bounce back from the objects in the path, bats listen to those echoes. Bats can vary the pulse frequency and the number of pulses produced per second; the pulse emission rate increases as the bats approach the prey. The loudness also varies with the pulse emissions, from loudest while searching for food to quieter as the prey is in proximity [49, 50]. Bats use the delay in the time of emissions, detection of echo, and variations in loudness to detect the orientation and distance of the prey, its type, and its speed. Bats have other sensitive senses like smell, and some even have good eyesight, but the BA is based on only echolocation. Figure 7 shows the bat algorithm working from the initialization of bats to the definition of the objective function, to the optimization of the function and respective adjustment of the parameters involved until the stopping criteria, are fulfilled. The population size, maximum and minimum values of the search space, the frequency range, loudness, and pulse emission rate (α) are some of the parameters that affect the optimization process in bat Algorithm. The careful selection of the hyperparameters for the BA is crucial for the algorithm's performance in optimization procedures. These hyperparameters have a noticeable impact on the algorithm's behavior as it moves through the convergence, exploration, and exploitation stages. The strength of the algorithm's exploration and exploitation efforts is influenced by the "loudness" parameter. The algorithm tends to explore new areas in the search space more thoroughly as "loudness" is increased.

3.4. Data Development and Analysis. A database comprised of 610 flat slab samples is curated from the published literature to predict the punching strength of slabs and the experimental setup used for the testing is shown in Figure 8. The dataset includes the following input parameters: slab depth

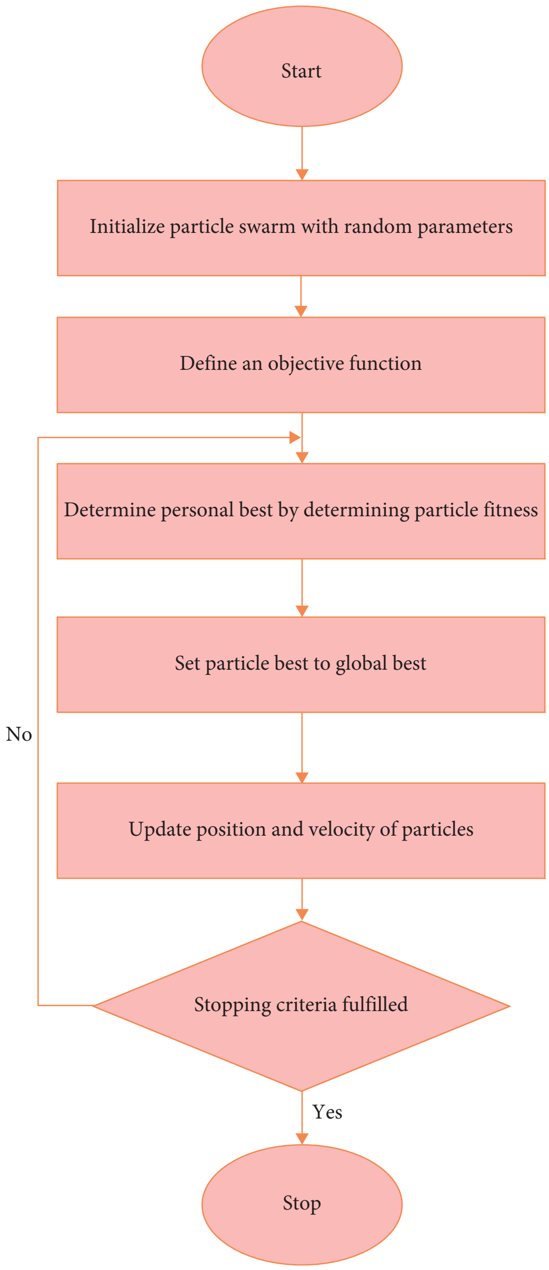

Figure 6: PSO flowchart.

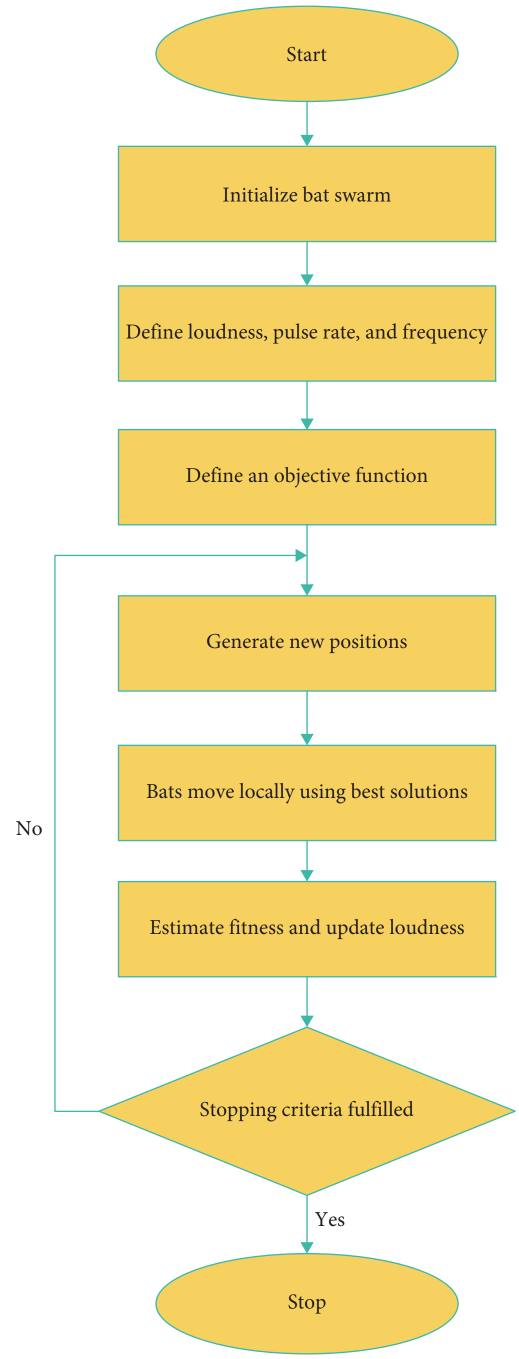

Figure 7: BA flowchart.

(d_s), column dimension (c_s), shear span ratio of flat slab (a_v/d), longitudinal reinforcement yield strength (f_y), longitudinal reinforcement ratio (ρ_l), ultimate load carrying capacity (V_u), and concrete compressive strength (f_c). The critical parameters are selected based on the physical models of CDCs. The statistical analysis of the dataset parameters including the minimum, maximum values, average, standard deviation, and covariance is given in Table 1 [42, 51]. The distribution of data in each parameter is represented by histograms, as shown in Figure 9. These histograms represent the variation of data used in experimental setups to measure the punching shear strength of the slab. The dataset provides several observations related to the experimental setup parameters and the resulting punching shear strength. Almost all parameters show a left-skewed distribution with only yield strength displaying a near-normal distribution. In almost all parameters, maximum data are present in the first one-third portion of the data, including 400 values of b less than 942.45 mm, 594 values of d less than 219 mm, 563 values of c less than 300 mm, 573 values of ρ less than 2.37%, 493 values of f_c less than 43.1 MPa, and 598 values of V_u less than 1,625 kN. The relationship between parameters was analyzed using Pearson's correlation coefficient revealing the influence of a parameter on each other, as shown in Figure 10. It is evident from the heatmap in

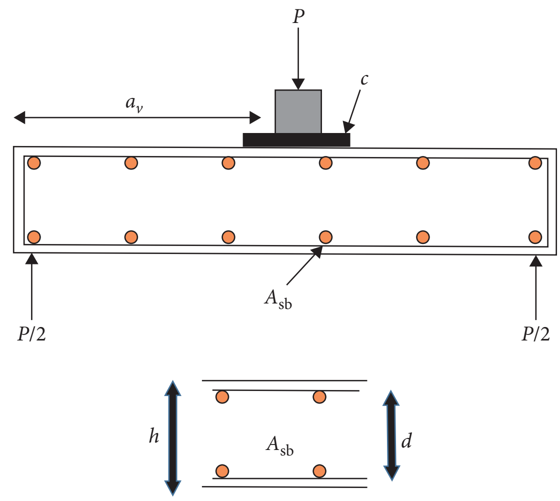

Figure 8: SCS experimental setup.

Table 1: Parametric details of SCS database.

Parameter	Unit	Minimum	Maximum	Difference	Avg.	St. dev	COVID-19
c_s	mm	50	901	851	204.986	104.747	0.511
d_s	mm	29.97	668.5	638.53	113.748	58.479	0.514
a_v/d	—	1.23	34	32.77	7.515	4.974	0.662
ρ_l	%	0.25	7.31	7.06	1.266	0.705	0.556
f_y	MPa	234.7	749	514.3	456.600	115.74	0.253
f_c	MPa	9.401	130.1	120.699	35.398	18.551	0.524
V_u	kN	24	4,915	4,891	403.258	406.229	1.007
M_f	kN mm	1	4,286	4,285	96.378	224.706	2.331

Figure 10 that significantly influenced by three geometric parameters including the parameter of the column, depth of slab, dimension of column, and two material properties including the yield strength of longitudinal reinforcement and compressive strength of the concrete. However, the geometric properties dominate the material properties. The correlation influence is represented by the intensity of color in the heatmap accompanied by correlation coefficient values. The dark color represents a strong correlation and a correlation value closer to +1, while a light color represents a weaker correlation with a correlation coefficient closer to 0 [42, 51].

3.5. Normalization of Data. Normalizing the database increases the efficiency of the ANN and the data can be denormalized at the end. Normalization helps in the conversion of data to unitless values that aid in making a visual correlation between data samples easier. Additionally, ANN shows low learning rates for unnormalized values [52–54]; therefore, normalizing the values between suitable upper and lower boundary values is a better practice. The normalization can be done by either using the built-in functions of the programming package or manually. Doing it manually provides better control over the normalization process, like using different upper and lower limits. The data were initially normalized between two sets of different extreme values including 0, 1, and 0.1, 0.9. But from the performance of the prediction models, it has been observed that values normalized between 0 and 1 resulted in better results. The data are normalized between 0 and 1 using Equation (8):

$$X = \frac{X_o - X_{\min}}{X_{\max} - X_{\min}}, \tag{8}$$

where $X_{\max}$ and $X_{\min}$ are the respective maximum and minimum values of the variable and X_o is the current value that is normalized to X.

3.6. Prediction Models. Several error metrics like mean squared error (MSE), MAE, and Pearson correlation coefficient (R^2) are used for selecting the ANN model [36]. The ANN model with the least values for MSE, MAE, and highest value for the R is used to train and test the dataset. ANN used for the database training and testing is MFNN, coded in MATLAB [35]. The hybrid models of PSOFNN and BATFNN use an objective function for optimizing the research problem. The objective function is optimized to maximize or minimize the fitness value of the hybrid model. For this study, MSE is used as an objective function in hybrid models. The analytical expression for the MSE is given by Equation (9):

$$\mathrm{MSE} = \sum_{i=1}^{n} \frac{(Y - \hat{Y})^2}{n}, \tag{9}$$

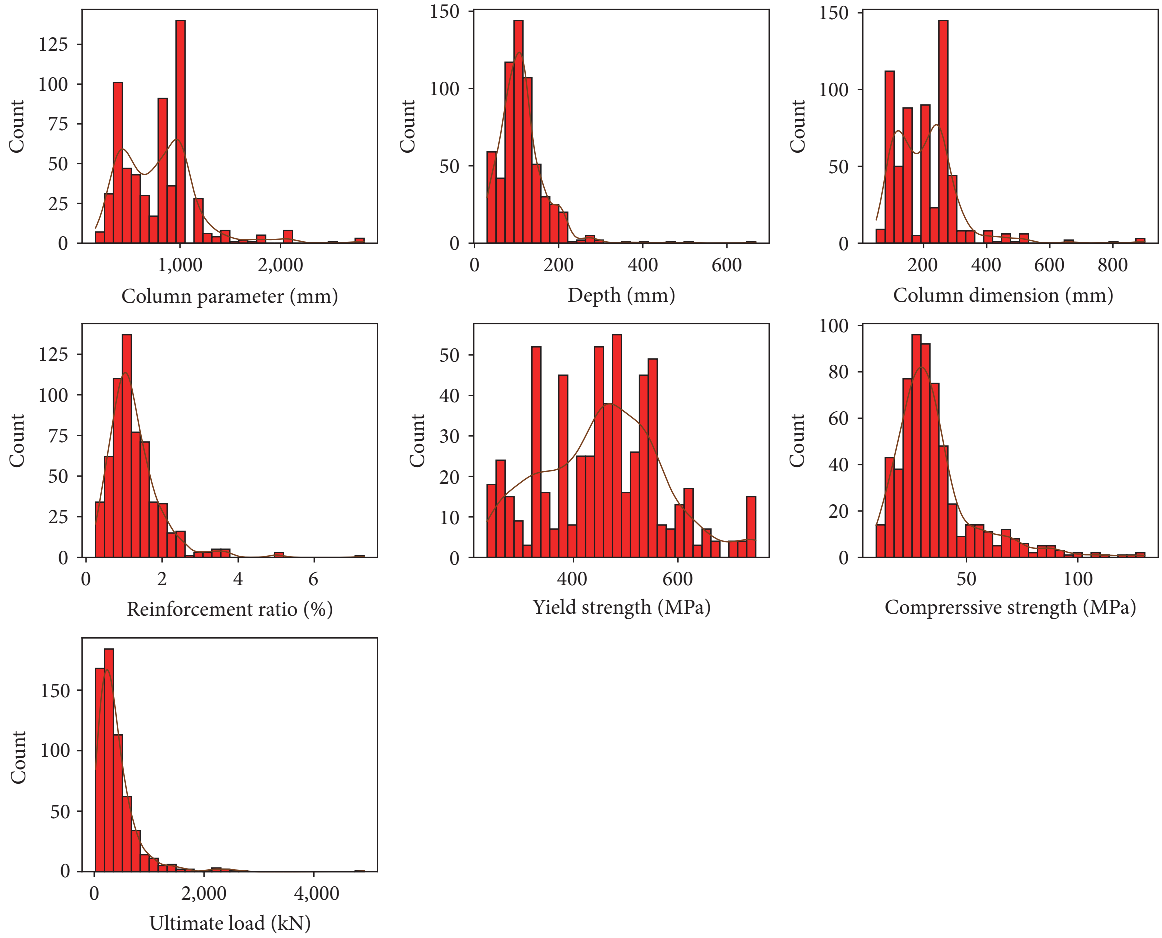

FIGURE 9: Correlation histogram for all parameters.

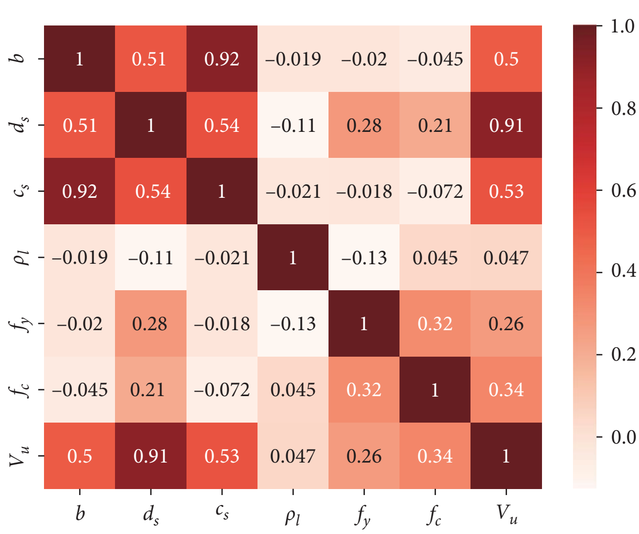

FIGURE 10: Correlation heatmap for all parameters.

where Y denotes the original target values, $\hat{Y}$ represents the predicted values of the target variable, and n is the total number of available samples.

The hybrid models and the ANN model resulting in the lowest value for the MSE, MAE, and the highest value for R is utilized for training and testing of data. The parameters for the hybrid models are selected based on the output values of error metrics. The models are run iteratively using different values for each parameter, for determining the optimum values of the parameters in the PSOFNN and BATFNN. Important parameters for the PSO algorithm are swarm population, inertia weight, personal and global learning coefficient, number of iterations, and upper and lower bounds. For the bat algorithm, the critical parameters are number of bats, iterations, and constant for loudness and rate of pulse emission. The number of layers in FNN, number of particles, and the number of iterations in PSOFNN and BATFNN used for each dataset are given in Table 2. The variation of the parameters in the hybrid model can help in the training and testing of the data. One might assume that increasing the swarm population or the number of iterations for the optimization algorithm will increase the efficiency of the hybrid models, but this does not always work. The increase in the parameters does not always prove to be beneficial for the optimization of the objective function. Therefore, the real challenge is to vary the parametric values until you get the best combination. Sometimes, the optimization efficiency will be the highest at the beginning which will optimize the results by more than 90% in the first few epochs, but it will not show much change as the iterations proceed.

Table 2: Parametric combination for SCS dataset for ML models.

Number	Dataset name	ANN layers	PSOFNN members	PSOFNN iterations	BATFNN members	BATFNN iterations	Parametric combination
1.	SCS = 1	14	50	300	30	300	$\rho_l, f_y, f_c, c_s, d_s, a_v/d_s$
2.	SCS = 2	12	50	300	30	300	$M_f, f_c, c_s, d_s, a_v/d_s$
3.	SCS = 3	8	50	300	30	300	$M_f/f_c bd_s^2, c_s/d_s, a_v/d_s$
4.	SCS = 4	10	30	300	30	300	$\rho_l, f_c/\mathrm{f}_y, c_s/d_s, a_v/d_s$
5.	SCS = 5	10	50	300	25	300	$M_f/bd_s^2, f_c, d_s, a_v/d_s$
6.	SCS = 6	10	50	300	25	300	$M_f/f_c \mathrm{bd}_s^2, d_s, c_s/d_s, a_v/d_s$
7.	SCS = 7	12	30	300	25	300	$M_f/f_c bd_s^2, f_c, d_s, c_s/d_s, a_v/d_s$

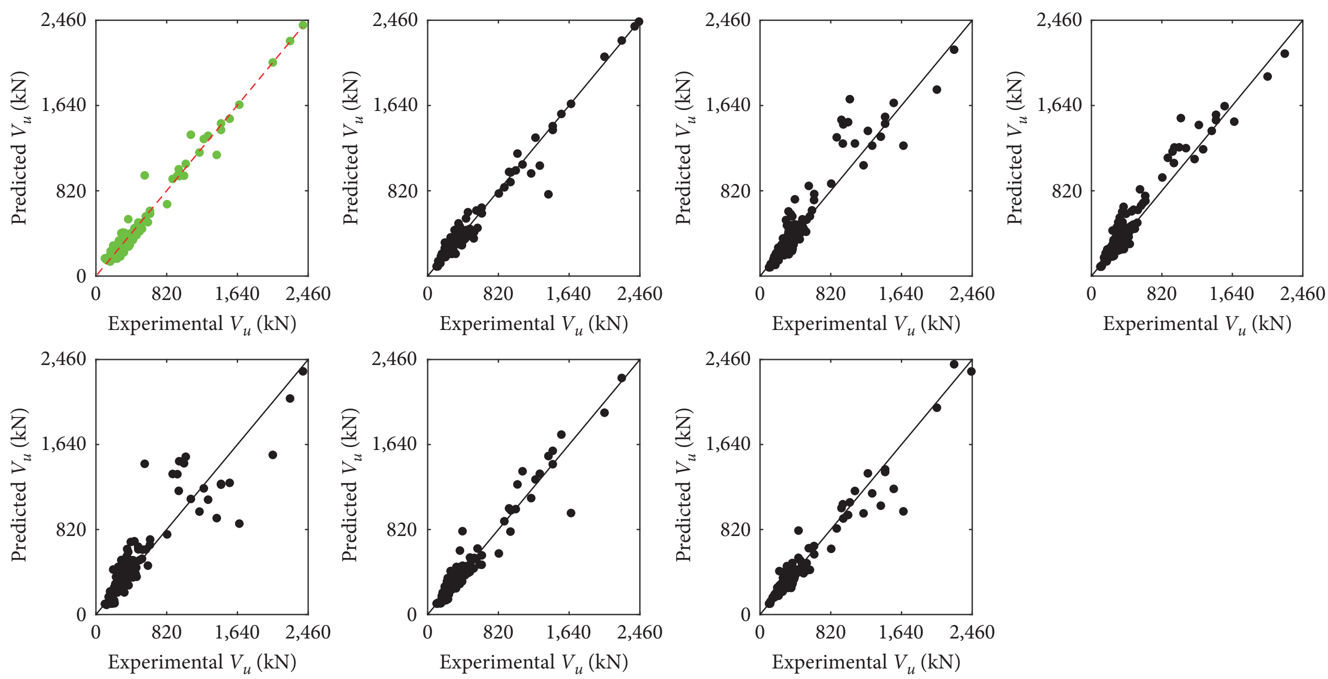

Figure 11: ANN-based predictions for shear strength.

4. Performance of ML Models

The flat slab dataset collected from published literature is converted to seven different subsets of data with different parameters taken from the original data. The seven subsets have different parameters, as shown in Table 2, that allow the determination of performance difference of the ML models with different parameters. All three ML models of ANN, PSOFNN, and BATFNN are trained on 465 samples and tested on 145 samples of each one of the seven subsets. The performance of these ML models is evaluated through three key parameters, including the R^2, MSE, and MAE, as discussed earlier. The predicted punching shear values of each ML model are visualized using scatter plots to understand the deviation of predicted and actual values for each sample. The scatter plots for test data of each subset are shown in Figures 11–16. The scatter plots with green-colored samples represent the best prediction accuracy of the respective ML model out of the seven subsets of data. ANN provided the best prediction of punching shear for the first subset of data with an accuracy of 98.5%. Additionally, the MSE and MAE values for the first subset of data were also the lowest from the error metrics of the other six subsets of data, as shown in Figure 12. This can be interpreted in a way that ANN understood the relationship between the parameters of the first subset and punching shear much better than in other subsets. Furthermore, the predicted punching shear values are closer to the experimental values for the first subset in ANN predictions, as shown in Figure 11.

The PSOFNN predictions for V_u represent that the predicted results of punching shear for the first and second subsets are better than the other five subsets of data. The MSE and MAE values for these two subsets are the lowest standing at 0.0275%, 1.214% for SCS = 1, and 0.0316%, 1.481% for SCS = 2, as shown in Figure 14. Based on the predicted values of the V_u, error metrics, and the R-value, PSOFNN for SCS = 1 is the best model having an R-value of 99.23%. The PSOFNN predicted values of punching shear for the first subset can be chosen as the best-predicted values of punching shear out of all three ML models. The scatter plot

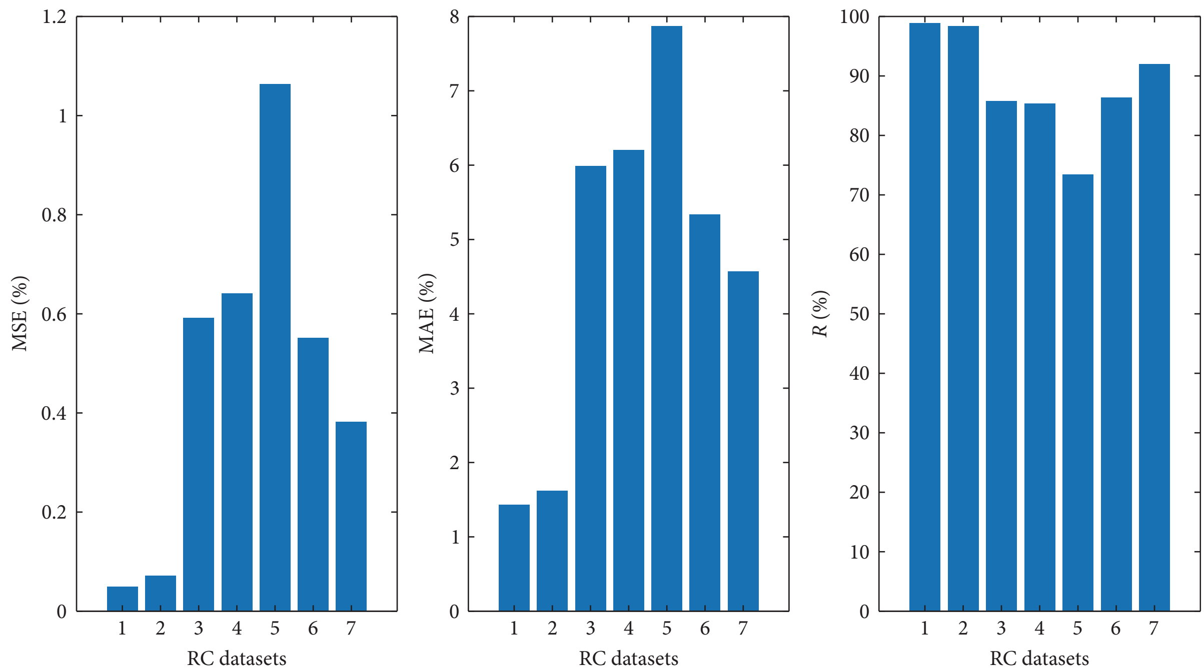

Figure 12: Error metrics for ANN.

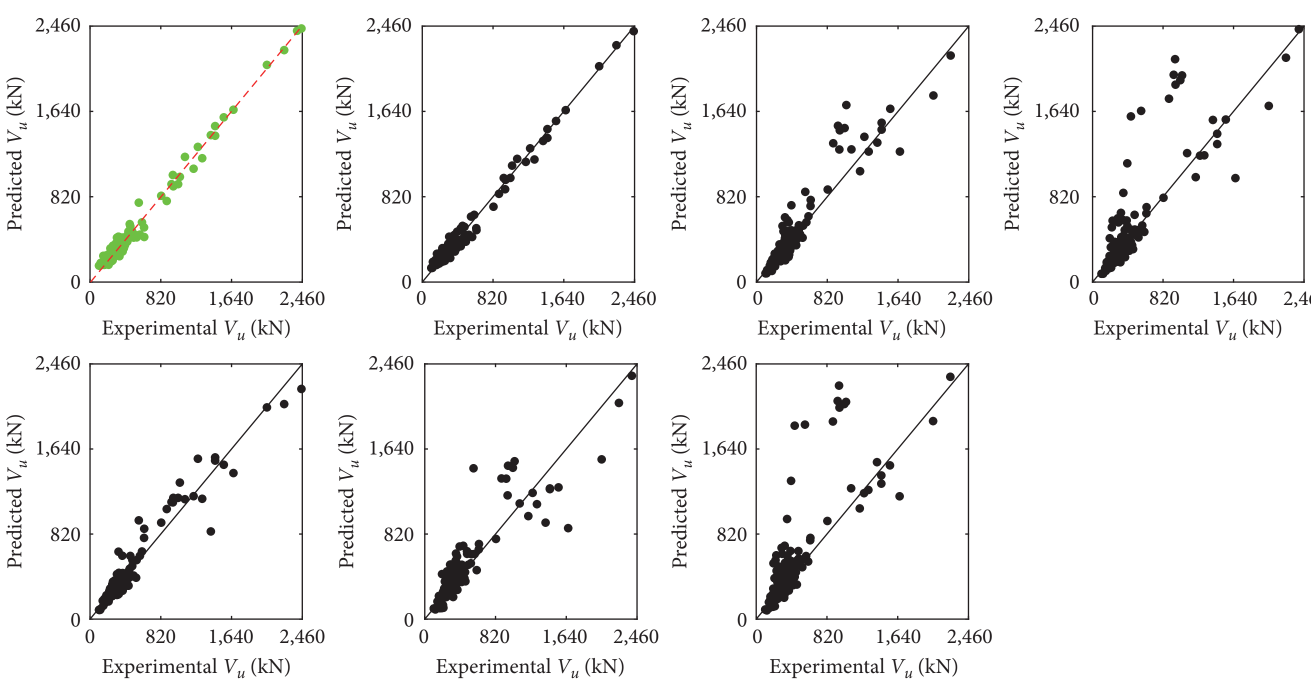

Figure 13: PSOFNN predictions of shear strength.

of PSOFNN and the visualizations of error metrics are shown in Figures 13 and 14. PSOFNN and ANN models also performed well with limited parameters as in the case of the third subset of data that has only four parameters. PSOFNN and ANN predicted the punching shear strength with an accuracy of 86.6% and 85.8%, respectively, using only four parameters. The PSOFNN model provided the lowest accuracy of 86.4% with the fifth subset of data while ANN dipped to an even lesser accuracy of 73.4% for this subset of data. The error metrics for the PSOFNN are lower than the error metrics of two other ML models for all seven subsets of the dataset.

ANN is the second-best model among the three ML models, while the BATFNN results show that the BAT algorithm does not properly optimize the objective function of MSE, as shown in the scatter plots and error metrics of Figures 15 and 16, respectively. BATFNN provided less

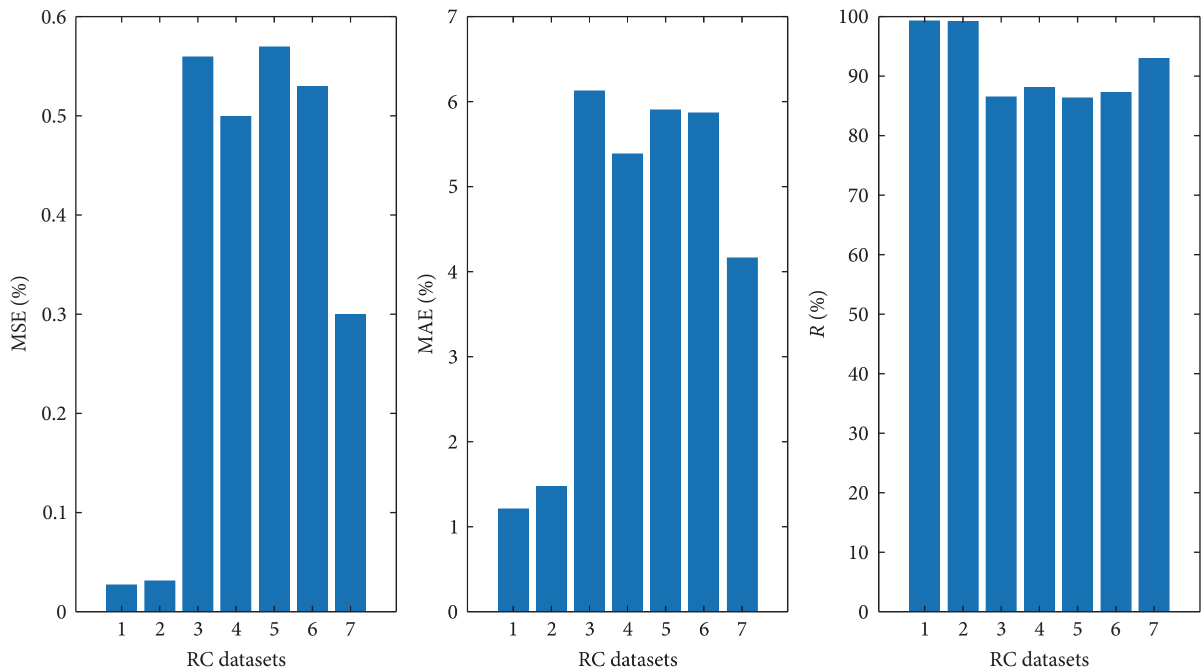

Figure 14: Error metrics for PSOFNN.

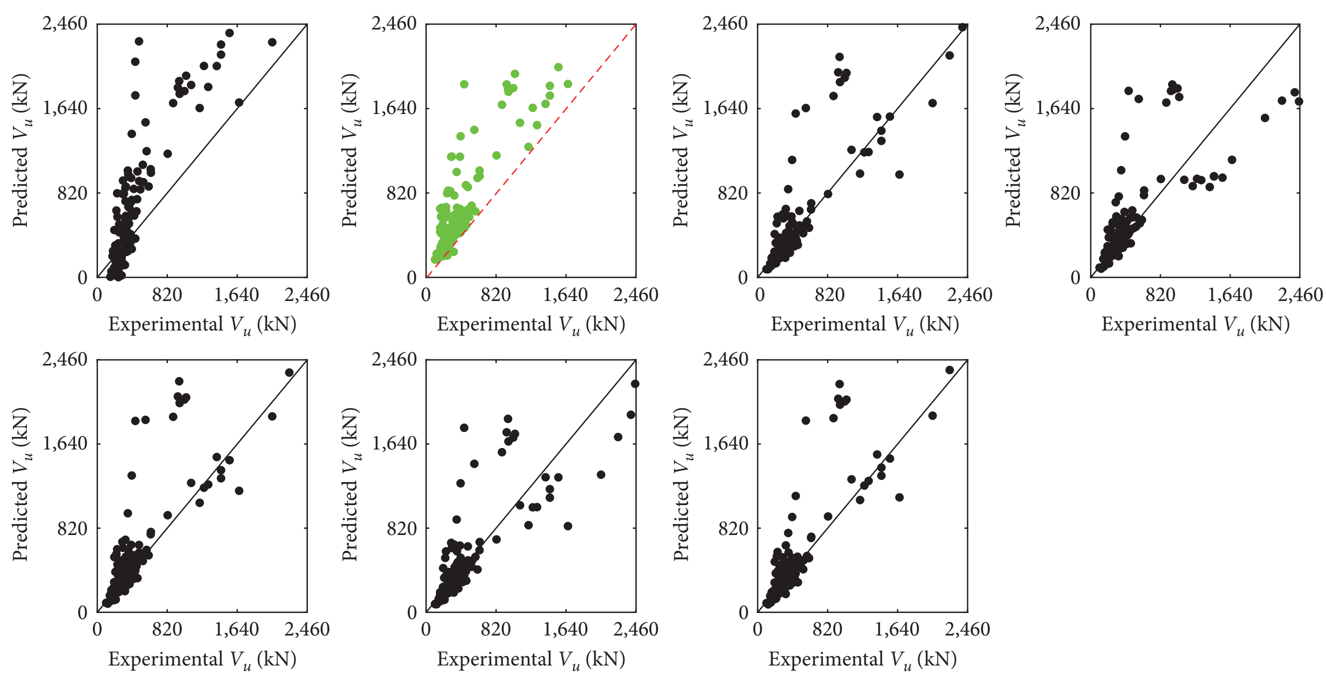

Figure 15: BATFNN predictions for shear strength.

accurate prediction results as compared to both ANN and PSOFNN. The predicted results of punching shear are also more dispersed than the other two models. The prediction results of ANN and PSOFNN are better for punching shear values less than 820 kN and the dispersion of predicted values increases on the subsequent values. However, the prediction of BATFNN shows greater dispersion under 820 kN even for the best performing BATFNN model on the second subset. Overall, based on all these observations, error metrics, and performance of models, the best prediction performance of PSOFNN among all ML models can be verified. From these results, one misconception that exists among novice researchers can be overruled that hybrid ANN models of metaheuristics outperform traditional ML models. The performance of two metaheuristic models of PSOFNN and BATFNN varied significantly from each other and ANN. The use of any metaheuristic

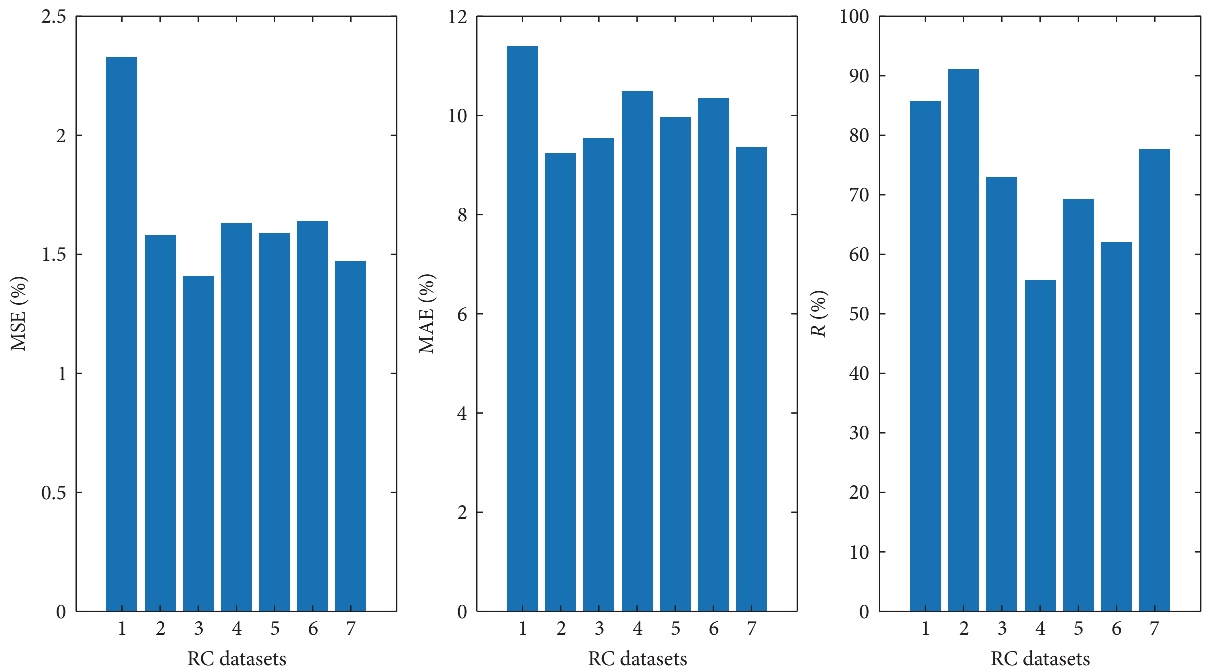

Figure 16: Error metrics for BATFNN.

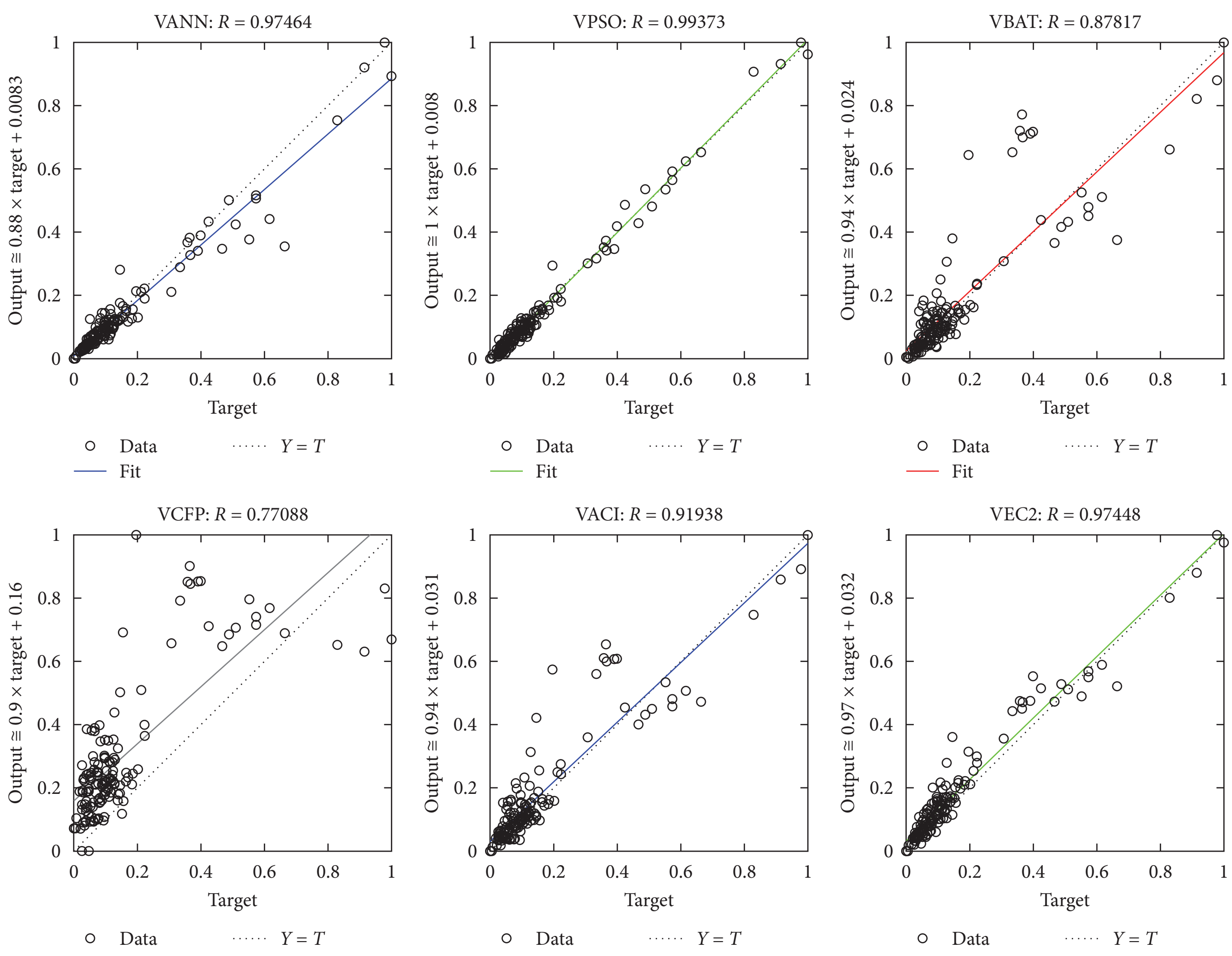

Figure 17: Value of R for six models.

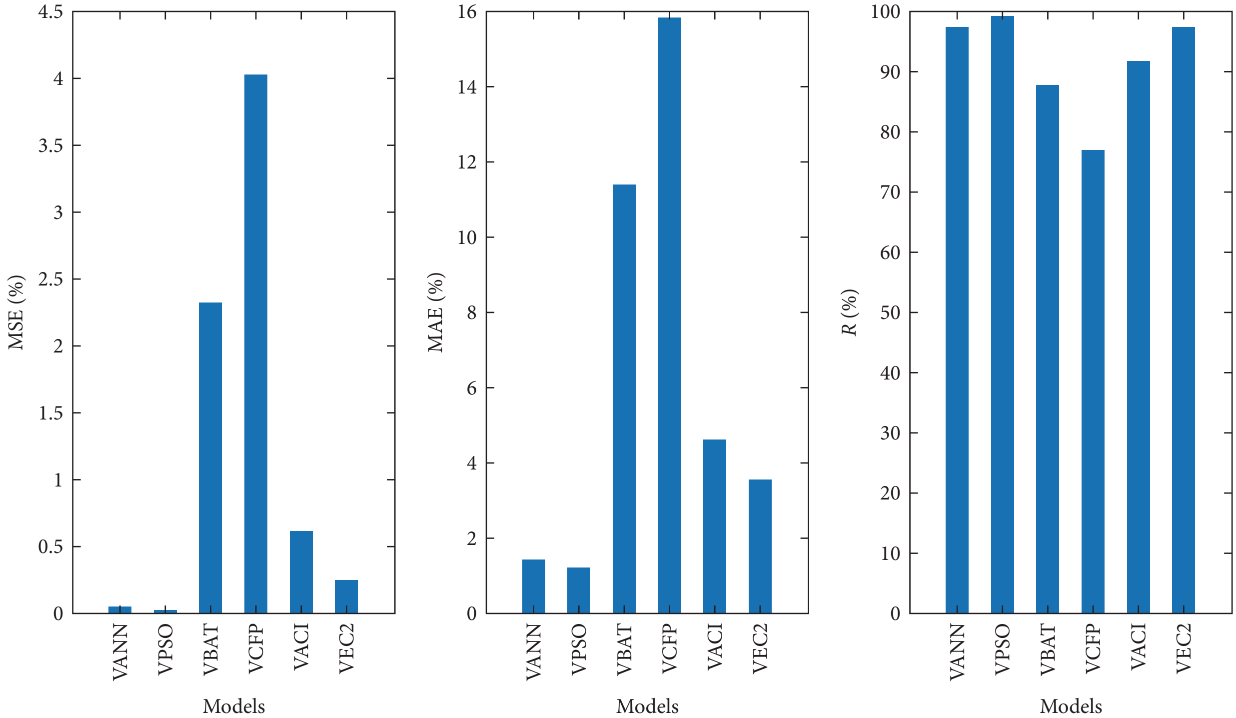

FIGURE 18: MSE, MAE, and R for six models.

model is not a universal solution to all optimization problems; therefore, this study recommends exploring the use of multiple metaheuristic models in a research study and evaluating their performance with the traditional ML models.

5. Comparative Studies of ML Models, CFP, and CDCs

In this section, a comprehensive analysis of the results obtained from six different approaches used for the shear strength prediction at slab–column connection is provided. These six approaches include the use of CDCs of ACI 318-19 and EC2, CFP, and three neural network-based models including FNN, PSOFNN, and BATFNN. The performance of each model is assessed using three key metrics including MSE, MAE, and R^2. These evaluation metrics provide information about the accuracy, precision, and fitness of models compared to the experimental values in the dataset. A thorough analysis shows that PSOFNN is the most reliable model for shear strength prediction of flat slabs, and it outperforms all other models in every evaluation metric and variation of the dataset. The PSOFNN provided the lowest values for the error metrics and the highest value for R^2. It should be noted that the design codes of ACI 318-19 underestimate the punching shear of a flat slab while EC2 overestimates [55]. In a comparison of design codes, it is observed that EC2 demonstrated a higher accuracy in representing the experimental results than the ACI 318-19 and the error metrics of the EC2 were also lesser than for the ACI 318-19. The best prediction results of each model are shown in Figure 17 and the error metrics including MSE, MAE, and R^2 for each model are shown in Figure 18. From these results, it becomes evident that PSOFNN is the best model for the prediction of punching shear strength of flat slabs with an R^2 value of 99.37%, MSE of 0.0275%, and MAE of 1.214%. The value of error metrics of MSE and MAE of punching shear results of EC2 is less than the error metrics of ACI 318-19 punching shear values. Abdallah et al. [56] analyzed the performance of three design codes including ACI 318-19, EC2, and British Standard (BS 8110-97). The study reported that EC2 performed better than ACI 318-19 and BS 8110-97 in predicting the punching shear of a flat slab. The CFP approach provided the least accurate punching shear values, with R^2 of only 77% and the highest MSE and MAE of 4% and 15.8%, respectively.

The normal distribution of the shear strength ratios for all models is shown in Figure 19. The shear strength ratio plot for the machine learning models of FNN, PSOFNN, and BATFNN are distributed uniformly around 1, and the width of their distribution curve is narrow suggesting that the shear strength ratios for these models are less dispersed and are closely clustered around the mean indicating good prediction results. In contrast, a wider curve or higher standard deviation of the shear strength ratio results for the other models including CFP, ACI 318-19, and EC2 indicate greater dispersion of values from the mean. The range of the ratio of experimental and predicted shear strength values for all models is given in Figure 20. This analysis suggests that PSOFNN stands out as the best model overall while EC2 demonstrates a superior performance in the domain of design codes.

6. Analysis of Results for Different Parameters

The effect of flat slab parameters on the prediction results of the CFP method, CDCs, ANN, PSOFNN, and BATFNN is

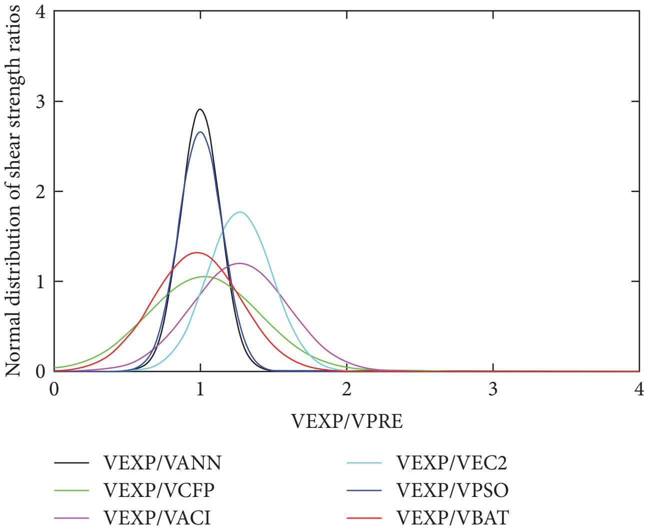

Figure 19: Normal distribution of shear strength ratios.

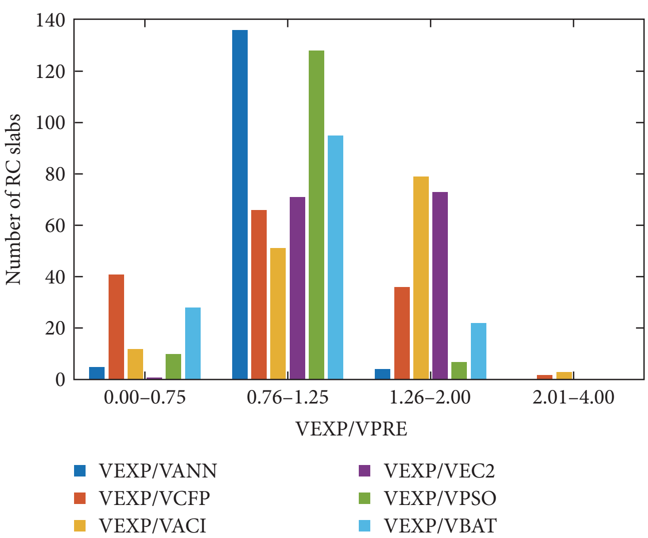

Figure 20: Range limit for SCS ratios.

discussed here. The parameters used for the parametric studies are slab depth (d_s), column dimension (c_s), shear span ratio of the flat slab (a_v/d), longitudinal reinforcement yield strength (f_y), longitudinal reinforcement ratio (ρ_l), ultimate load-carrying capacity (V_u), and concrete compressive strength (f_c). The parametric study was done to determine the influence of these parameters on the ratio of VEXP/VPRED.

6.1. Effective Depth of Slab (d_s). The plots for the prediction of SCS punching failure response, as illustrated in Figure 21, show that the effective slab depth (d_s) is one of the most influential geometric features for flat slab punching failure. According to a research study by Liang et al. [57], the punching shear strength of a flat slab increased with an increase in the effective depth of the slab in agreement with the findings of this study. Lapi et al. [58] applied a concrete overlay as a retrofitting technique against the punching failure of a flat slab. The researchers reported a significant enhancement in the punching resistance of flat slabs. The results of our study show that the parametric comparative analysis for PSOFNN is better than the ANN, BATFNN, CDCs, and CFP. The results of PSOFNN and ANN are closer to the experimental value of ratios and the unity line is used as a reference for determining the fit of the ratios. The plots of the CDCs ratio in Figure 21 against d_s show that most of the values are above the unity line, indicating that CDCs result in values lesser than actual experimental values. The scatter of points for the PSOFNN is closer to the unity line, as shown in Figure 21, indicating that PSOFNN predicted values are closer to the experimental values. The results can be used to further analyze the reason that results in lesser values for shear strength than actual. The values of d_s in the range of 75 –135 mm showed the highest deviation from the unity line. This requires revising the CDCs as they are not accurately predicting the values of the punching shear, this means that the actual punching shear at the column–slab connection is larger than the values calculated using CDCs, which can lead to punching shear failure.

6.2. Shear Span Ratio (a_v/d). The effect of shear punching failure in flat slabs is studied for the experimental and predicted values ratio against the shear span ratio of flat slabs. The scatter of ratios on the unity line in Figure 22 shows that the values are closer to the unity line for the PSOFNN and ANN, and the scatter is also uniform on the top and below of unity line for ANN, PSOFNN, BATFNN, and CFP. Although the values of the ratio are scattered more widely for the CFP that there is no clear bias toward underestimation or overestimation of values. ACI and EC2 codes show the highest biases of values of ratios toward lesser values than the original, as shown in Figure 22.

6.3. Compressive Strength (f_c). For the flat slabs, punching failure can be predicted more precisely by using compressive strength (f_c) [57], as illustrated in Figure 23. It has been reported by numerous research studies [6, 59, 60] that the compressive strength of concrete has a profound influence on the punching shear of flat slab. The results of the PSOFNN and ANN are close to the experimental results; therefore, the scatter of the points is close to the unity line, while the scatter of VEXP/VACI and VEXP/VEC2 against the unity line show that ACI underestimate and EC2 overestimate the values that are in agreement with the previous findings [55]. The ideal case requires these values to lie on the unity line but the presence of most points above the unity line is proof that values calculated by the CDCs are less than the actual experimental values. The highest deviation resulted from the values in the range of 2040 MPa for f_c. The scatter of points in the CFP and BATFNN plots in Figure 23 show that the values for these two are roughly uniformly distributed around the unity line. This indicates the nonbiasedness of these two approaches toward overestimation or underestimation of the values.

6.4. Longitudinal Reinforcement Ratio (ρ_l). The flat slab samples having the reinforcement ratio value between 1.5% and 2.5% show the most deviation from the unity line, as shown

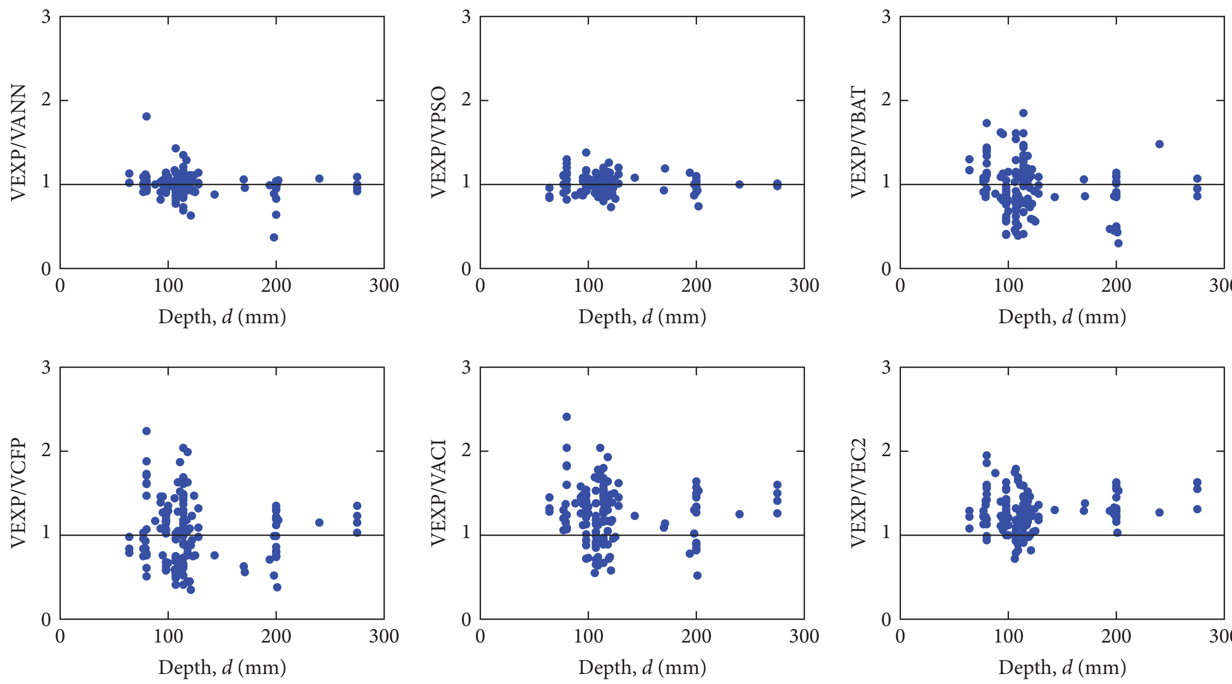

Figure 21: Shear strength ratio against depth.

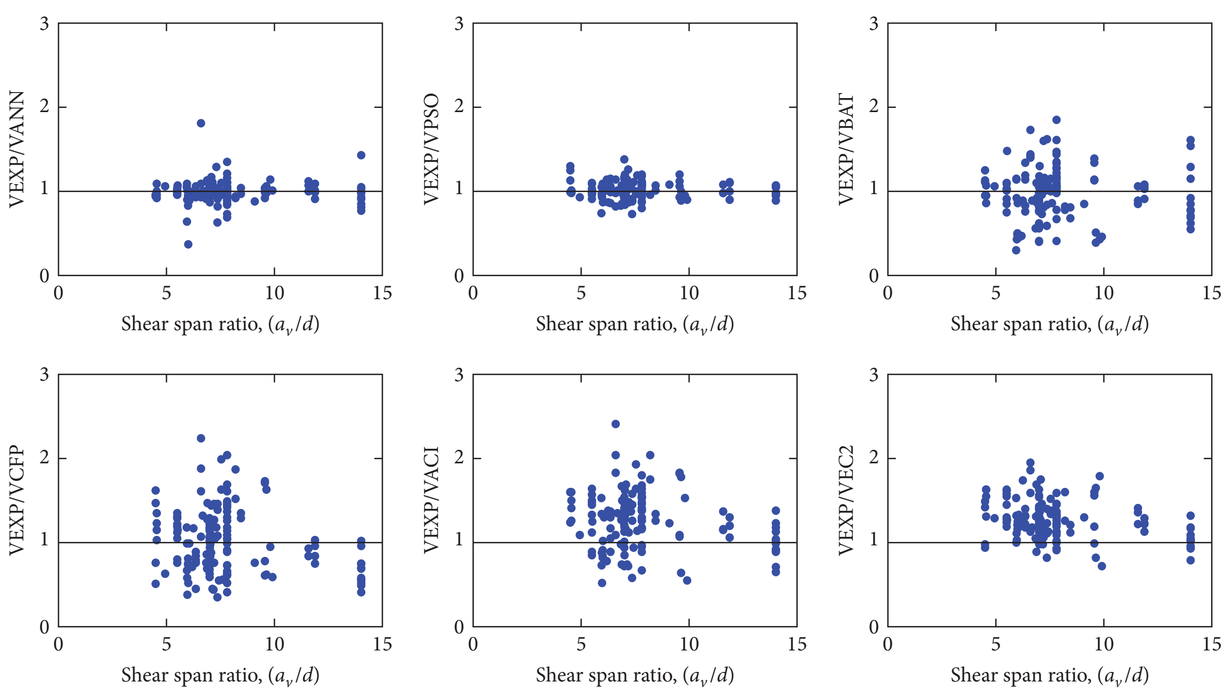

Figure 22: Shear strength ratio against span ratio.

in Figure 24. The reinforcement ratio is one of the two most important material properties for the prediction of the punching shear failure response of a flat slab and it has a positive influence on the punching shear strength of a flat slab [61]. Marzouk and Hussein [62] reported an increase in the punching shear strength of flat slabs with an increase in the quantity of reinforcement. Shen et al. [63] reported longitudinal reinforcement as the most influential factor in predicting the punching shear of a flat slab. The scatter of the points is closer to the unity line for the PSOFNN and ANN which shows that the PSOFNN and ANN have performed better predictions than the rest of the four models. The BATFNN has performed less accurate predictions than PSOFNN and ANN, but the results are less scattered than the CFP and ACI

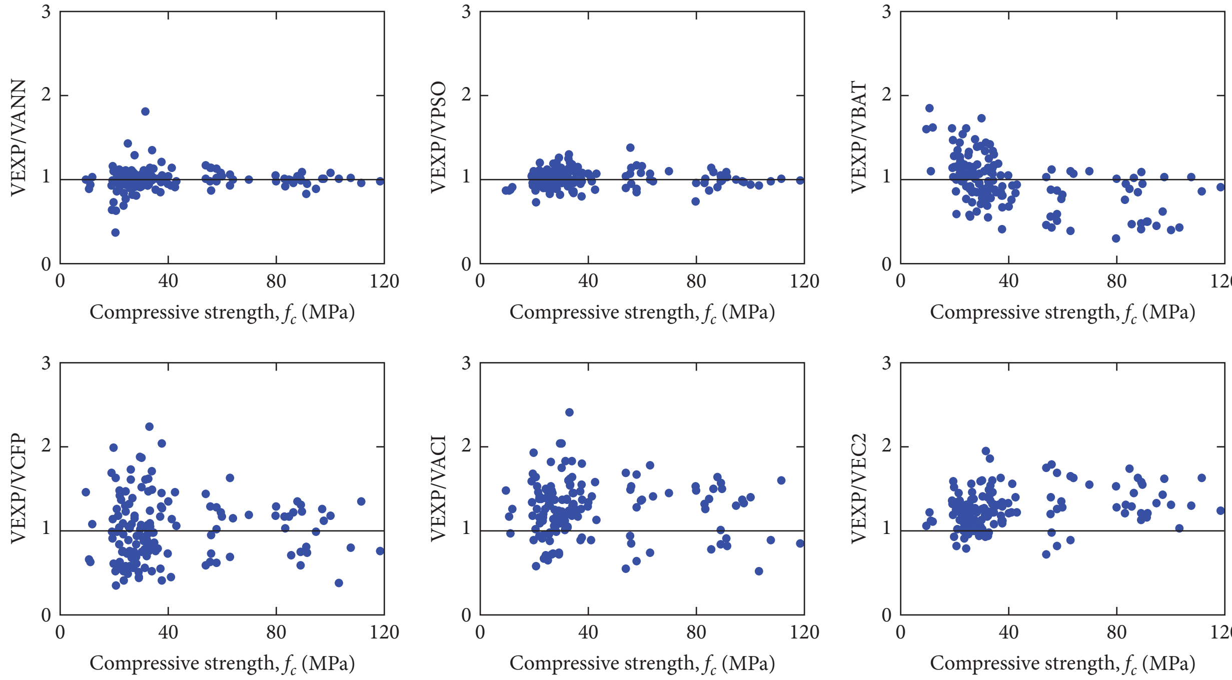

Figure 23: Shear strength ratio against compressive strength.

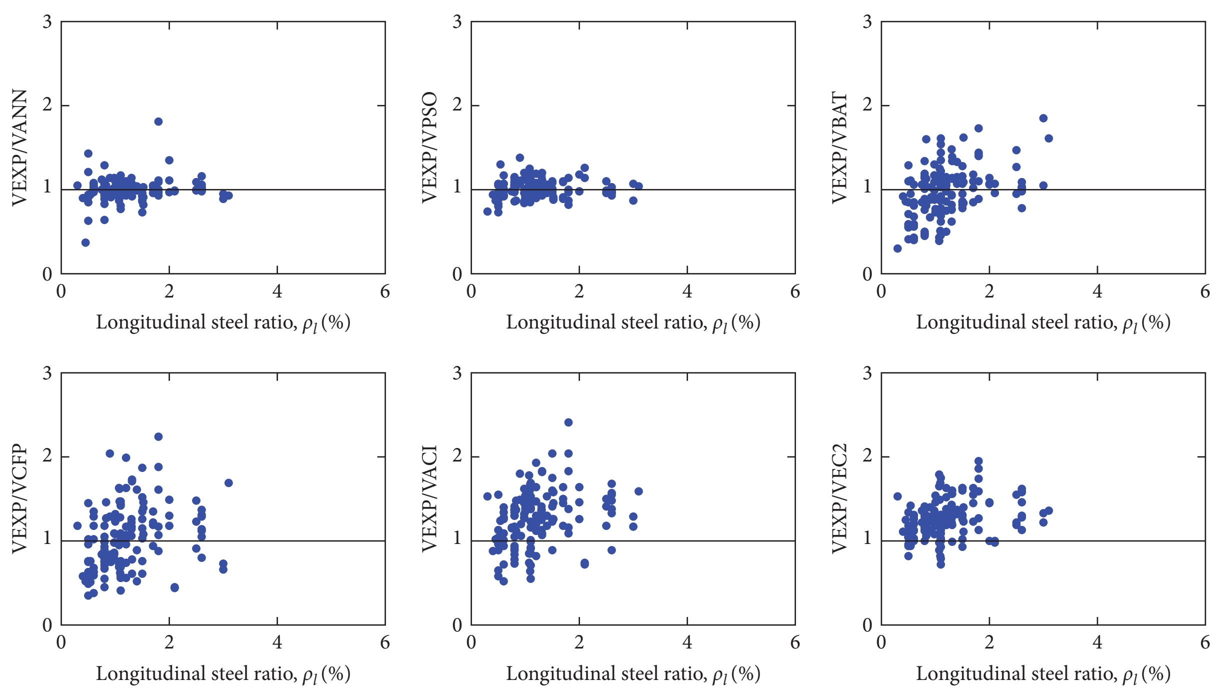

Figure 24: Shear strength ratio against longitudinal steel ratio.

codes. In addition, the ANN, PSOFNN, and BATFNN have shown no bias in predicting the punching shear strength either toward underestimation or overestimation.

7. Using NLFEA for RC Flat Slab Assessment

The behavior of concrete is nonlinear, and in Abaqus, this behavior is studied using the concrete-damaged plasticity and smeared crack model. The compression and tension region in concrete or the biaxial tension region results in the cracking of concrete at the failure in case of smeared crack concrete modeling [33, 51, 64, 65]. The smeared crack modeling is used for representing concrete crushing due to compression or cracking because of tension, respectively. Under uniaxial tensile loading, concrete behaves elastically for as long as the tensile loading is in the range of 7.5%–11%

Table 3: ABAQUS CDP model parameters.

Description	Used value
Dilation angle (ψ)	35° (calibrated)
Eccentricity (ε)	0.1 (default)
Shape factor (K_c)	0.667 (default)
Stress ratio (σ_{b0}/σ_{c0})	1.16 (default)
Viscosity parameter	0.0003 (calibrated)

Table 4: Selected samples for SCS.

Source	Name	d_s (mm)	c_s (mm)	a_{vs}/d_s	f_{cs} (MPa)	f_{ys} (MPa)	ρ_{ls} (%)
Kotsovos [66]	S1	205	255	6.2	24.25	655	0.085
Kotsovos [66]	S3	205	255	6.2	24.25	665	0.345
Caldentey et al. [67]	C1	255	455	5.6	33.95	555	1.075

of final compressive stress, after this, the concrete cracking begins. It is assumed that cracking will occur when the stress in concrete approaches the failure surface is known as the "crack detection surface." The cracking damages the structure, and the smeared cracking model also considers the cracking as damage. The cracks under compressive stress are considered to be completely closed because these types of cracks do not show any strain.

7.1. Concrete Damaged Plasticity Model. In ABAQUS, the behavior of concrete material in the inelastic range is defined using the concrete-damaged plasticity model. This model can be used for plain concrete, but its main purpose is to analyze RC. Concrete subjected to low confining pressures or monotonic and cycling loading can be analyzed using this model. The model considers two main failure mechanisms of concrete, one by crushing concrete and another by tensile cracking. Under the action of uniaxial tensile stresses, the stress and strain follow a linear elastic relationship till failure occurs. As the tensile stresses increase beyond the failure stress, strain localization occurs in the concrete. When the uniaxial compression is applied, the response is linear till the initial yield point leading to a stress-hardening state in the plastic region that causes strain softening as the stresses increase beyond ultimate stress. The behavior of concrete is brittle under low confining pressures and the CDP model represents this failure using stress and plastic strain.

The nonlinear behavior of concrete slabs is studied using ABAQUS. A quarter portion of the slab is modeled and analyzed in ABAQUS to reduce the analysis time required for the analysis of the full slab. The continuity condition is fulfilled using the boundary condition for the quarter portion of the slab. Several important material and geometric parameters are used to calibrate the slab model including the size of the mesh, dilation angle, eccentricity, viscosity, uniaxial to biaxial stress ratio, and various element types of concrete and steel. Load deflection curves are plotted with MATLAB using the results obtained from the load–displacement analysis of the slab.

The elastic stiffness of the sample undergoes degradation when it is unloaded in the strain-softening region of stress and strain curves. The stress–strain relationship under the action of uniaxial compression and tension is calculated by using Equations (10) and (11):

$$\sigma_c = (1 - d_c)E_o(\varepsilon_c^{\sim \mathrm{in}} - \varepsilon_c^{\sim \rho_l}), \tag{10}$$

$$\sigma_t = (1 - d_t)E_o(\varepsilon_t^{\sim \mathrm{in}} - \varepsilon_t^{\sim \rho_l}). \tag{11}$$

The damage in the elastic stiffness is represented by two variables d_t and d_c, whose value depends on the temperature, plastic strain, and field parameters involved. The value of these damage variables varies from 0 to 1, representing no damage and complete strength loss, respectively. The other parameters involved in the equations are the initial elastic stiffness of the material (E_o), compressive strain (ε_c), tensile strain (ε_t), and the superscripts $\sim$in and $\sim\rho_l$ represent inelastic strain and plastic strain, respectively. The concrete damaged plasticity model is used to model the plastic behavior of concrete using various parameters involving dilation angle, viscosity, load eccentricity, ratio of uniaxial to biaxial stress, and shape factor of yielding surface, based on the author's previous experience, as mentioned in Table 3.

These data have been used to perform FEA of some selected cases of flat slab that are mentioned in Table 4. The tension stiffening simulation is defined in the slab model to represent the strain-softening behavior of cracked concrete. This tension stiffening is specified in one of two ways either by using a fracture energy cracking criterion or the stress–strain relationship of concrete after failure.

In ABAQUS, the steel bars and concrete are considered to be perfectly bonded. ABAQUS uses truss elements to represent the steel bars having two nodes with three translations at each. The material properties used for steel bars are yield strength, modulus of elasticity, and Poisson's ratio with respective values of 420 MPa, 200 GPa, and 0.3. The results of the ML models are verified using the analysis results from ABAQUS. The load-deflection curves from ABAQUS are in

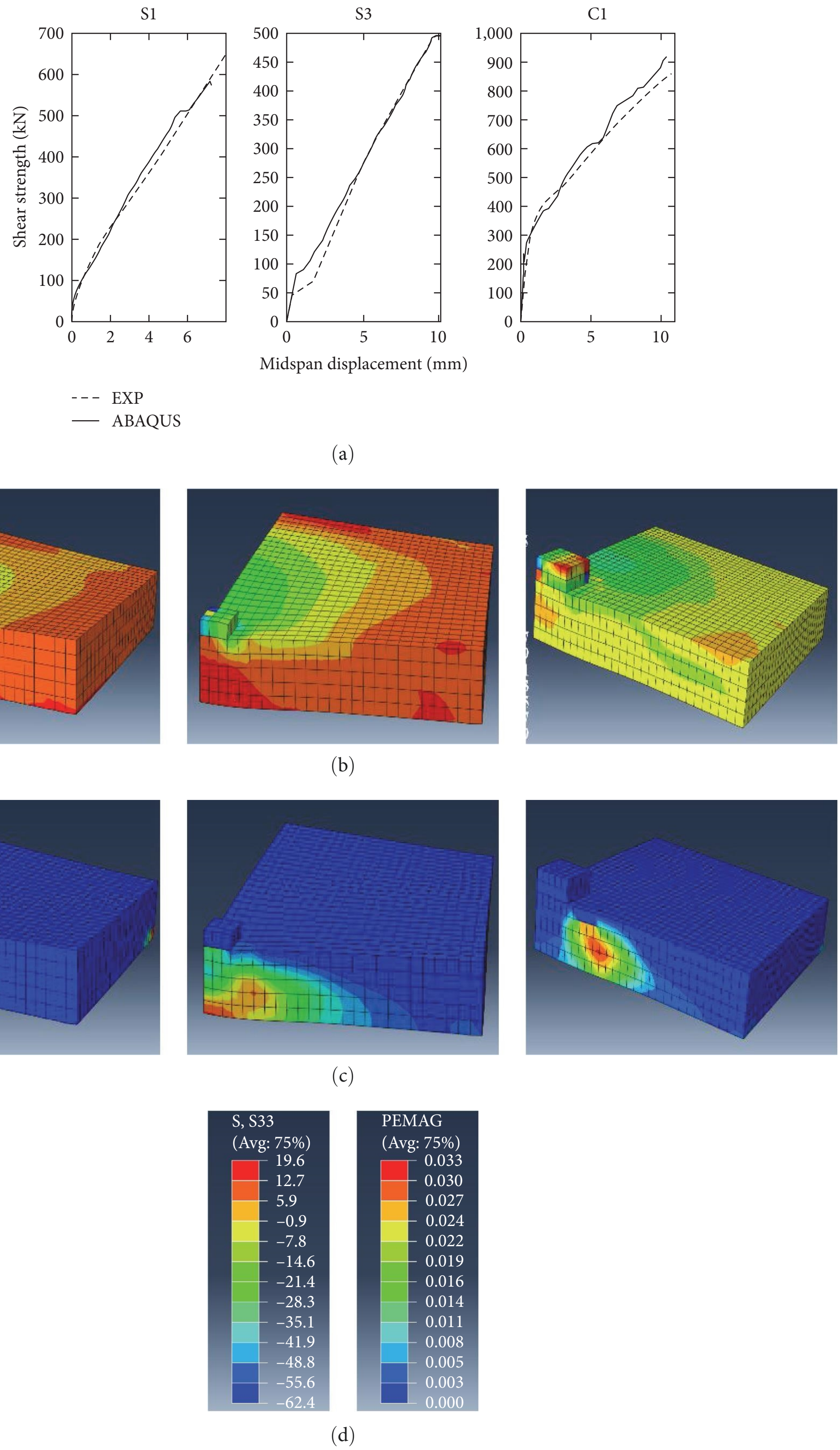

FIGURE 25: (a) LD curve, (b) S33, (c) PEMAG, and (d) LEGEND for SCS [42].

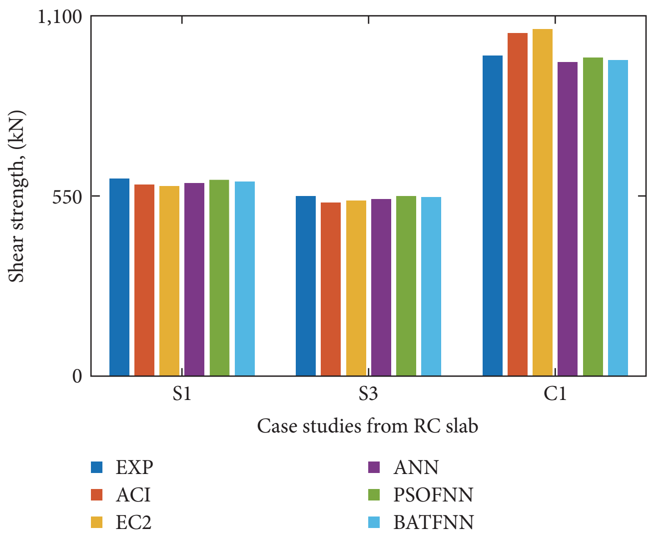

Figure 26: Comparison of design codes and hybrid models with experimental values of selected cases.

good relationship with the curves from experimental data, as shown in Figure 25(a).

Figure 26 compares the values of all prediction models with experimental values and design code. It has been observed that PSOFNN provided highly accurate prediction results for the flat slab punching shear values, between the three hybrid models. Furthermore, the PSOFNN also outperformed design codes, and the validation of FEA of flat slab provided good agreement with the findings of the PSOFNN model. Also, the comparison of design codes, EC2 is the best design code for the calculation of punching shear of a flat slab. Through the parametric analysis, it is found that ACI 318-19 has a slight tendency to underestimate the punching shear while EC2 overestimates the punching shear.

8. Conclusions

This research study investigates the influence of multiple subsets of data with different parameters on the performance of machine learning models to predict the punching shear of flat slabs. The motivation for the application of different ML models was to address the limitations in the existing design codes and provide a comparison of different ML models. Additionally, the study discusses the performance of two design codes including ACI 318-19, EC2, and an analytical approach of the CFP method. A database of square flat slabs consisting of 610 samples has been built from literature with parameters related to the slab depth, column dimension, shear span ratio of slab, yield strength of longitudinal steel, longitudinal reinforcement ratio, ultimate load carrying capacity, and compressive strength of concrete. Three ML models including ANN, PSOFNN, and BATFNN are employed in this database and their performance is assessed using three performance measures R^2, MSE, and MAE. After that a comprehensive comparison of the performance of ML models is provided, followed by the comparison of all empirical and prediction approaches in the next section. In the next section, the influence of some key parameters such as d_s, ρ_l, a_v/d, and f_c on the shear strength of flat slab is discussed and cross-referenced from previous literature to validate the findings of this study. Finally, the predicted shear strength values were also validated with the FEA of the flat slab in Abaqus. Based on these sections, the following main conclusions are summarized:

(1) From the comparison of prediction models, it has been observed that PSOFNN provided highly accurate prediction results for the flat slab punching shear values. It achieved impressive metrics, with R^2, MSE, and MAE values of 99.37%, 0.0275%, and 1.214%, respectively. The PSOFNN also outperformed design codes and the validation of FEA of flat slab provided good agreement with the findings of the PSOFNN model.

(2) In the comparison of design codes, EC2 is the best design code for the calculation of punching shear of a flat slab. Through the parametric analysis, it is found that ACI 318-19 has a slight tendency to underestimate the punching shear while EC2 overestimates the punching shear. However, the PSOFNN models do not show any bias toward either overestimation or underestimation of punching shear values.

(3) From the correlation, parametric analysis, and comparison of the performance of individual models on seven different subsets of data, several key parameters have been found that significantly influence the punching shear of a flat slab. It has been observed that the effective depth of the slab, column dimensions, yield strength of reinforcement, and compressive strength of concrete have the highest impact on the punching shear values. An increase in the depth of the slab either before construction or after construction through retrofitting results in enhanced punching shear resistance of the flat slab. Therefore, proper selection of geometrical properties of slab–column elements and material properties is crucial for improved performance of flat slabs against punching shear failure.

(4) Another important finding of this study is the use of multiple metaheuristic models on a single research problem. PSOFNN and BATFNN have shown significantly different results that show that not all hybrid models of metaheuristic algorithms-based neural networks can optimize on any research problem equally and not all of them can outperform ANN as usually perceived.

The study reveals that the empirical models are less accurate in predicting the punching shear strength of flat slabs which is a major concern since failure in flat slabs normally occurs due to punching failure at slab–column connection. This study shows that ML models tend to better accommodate the complex behavior of flat slabs; therefore, it is recommended that new research focuses on the use of ML models to develop empirical equations for punching shear strength of flat slabs using a dataset representative of large experimental research.

Data Availability

Data supporting this reasearch article are available on request.

Disclosure

The earlier version of it has been presented as "arxiv" according to the following link: "https://arxiv.org/abs/2311.12824," with complete reference of Wahab, S., Mahmoudabadi, N. S., Waqas, S., Herl, N., Iqbal, M., Alam, K., & Ahmad, A. (2023). Comparative analysis of shear strength prediction models for reinforced concrete slab–column connections. arXiv preprint arXiv:2311.12824.

Conflicts of Interest

The authors declare that they have no conflicts of interest.

Authors' Contributions

All authors have read and agreed to the published version of the manuscript.

References

[1] W. Piel and G. Hanswille, "Composite shear head systems for improved punching shear resistance of flat slabs," *Composite Construction in Steel and Concrete V*, pp. 226–235, 2012.

[2] P. Weerasinghe, K. Nguyen, P. Mendis, and M. Guerrieri, "Large-scale experiment on the behaviour of concrete flat slabs subjected to standard fire," *Journal of Building Engineering*, vol. 30, Article ID 101255, 2020.

[3] S. Amiri and S. Behzad Talaeitaba, "Punching shear strengthening of flat slabs with EBROG and EBRIG–FRP strips," *Structures*, vol. 26, pp. 139–155, 2020.

[4] N. Jafarian, D. Mostofinejad, and A. Naderi, "Effects of FRP grids on punching shear behavior of reinforced concrete slabs," *Structures*, vol. 28, pp. 2523–2536, 2020.

[5] C.-C. Chen and C.-Y. Li, "Punching shear strength of reinforced concrete slabs strengthened with glass fiber-reinforced polymer laminates," *Structural Journal*, vol. 102, no. 4, pp. 535–542, 2005.

[6] R. Z. Alrousan and B. R. Alnemrawi, "The influence of concrete compressive strength on the punching shear capacity of reinforced concrete flat slabs under different opening configurations and loading conditions," *Structures*, vol. 44, pp. 101–119, 2022.

[7] G. Birkle, *Flat slabs: the influence of the slab thickness and the stud layout*, Doctoral Thesis, University of Calgary, Calgary, Canada, 2004.

[8] R. T. S. Mabrouk, A. Bakr, and H. Abdalla, "Effect of flexural and shear reinforcement on the punching behavior of reinforced concrete flat slabs," *Alexandria Engineering Journal*, vol. 56, no. 4, pp. 591–599, 2017.

[9] J. Einpaul, C. E. Ospina, M. F. Ruiz, and A. Muttoni, "Punching shear capacity of continuous slabs," *ACI Structural Journal*, vol. 113, no. 4, pp. 861–872, 2016.

[10] S. Kinnunen and H. Nylander, *Punching of Concrete Slabs without Shear Reinforcement*, Elanders Boktryckeri Aktiebolag, Göteborg, 1960.

[11] I. A. E. M. Shehata, "Simplified model for estimating the punching resistance of reinforced corete slabs," *Materials and Structures*, vol. 23, no. 5, pp. 364–371, 1990.

[12] C. Européen, *Eurocode 2: Design of Concrete Structures—Part 1-1: General Rules and Rules for Buildings*, British Standard Institution, London, 2004.

[13] A. Committee, *Building Code Requirements for Structural Concrete (ACI 318-08) and Commentary*, American Concrete Institute, 2008.

[14] H. Marzouk, E. Rizk, and R. Tiller, "Design of shear reinforcement for thick plates using a strut-and-tie model," *Canadian Journal of Civil Engineering*, vol. 37, no. 2, pp. 181–194, 2010.

[15] A. S. A. Jabbar, M. A. Alam, and K. N. Mustapha, "A new equation for predicting punching shear strength of R/C flat plates," in *Proceedings National Graduate Conference 2012 (NatGrad2012)*, pp. 1–4, University Tenaga Nasional, Putrajaya Campus, November 2012.

[16] I. Alkroosh and H. Ammash, "Soft computing for modeling punching shear of reinforced concrete flat slabs," *Ain Shams Engineering Journal*, vol. 6, no. 2, pp. 439–448, 2015.

[17] A. Ahmad, G. Kotsovou, D. M. Cotsovos, and N. D. Lagaros, "Assessing the accuracy of RC design code predictions through the use of artificial neural networks," *International Journal of Advanced Structural Engineering*, vol. 10, no. 4, pp. 349–365, 2018.

[18] F. Demir, "Prediction of elastic modulus of normal and high strength concrete by artificial neural networks," *Construction and Building Materials*, vol. 22, no. 7, pp. 1428–1435, 2008.

[19] R. Perera, M. Barchín, A. Arteaga, and A. D. Diego, "Prediction of the ultimate strength of reinforced concrete beams FRP-strengthened in shear using neural networks," *Composites Part B: Engineering*, vol. 41, no. 4, pp. 287–298, 2010.

[20] G. H. Shafabakhsh, O. J. Ani, and M. Talebsafa, "Artificial neural network modeling (ANN) for predicting rutting performance of nano-modified hot-mix asphalt mixtures containing steel slag aggregates," *Construction and Building Materials*, vol. 85, pp. 136–143, 2015.

[21] M. Shariati, M. S. Mafipour, P. Mehrabi et al., "Application of a hybrid artificial neural network-particle swarm optimization (ANN-PSO) model in behavior prediction of channel shear connectors embedded in normal and high-strength concrete," *Applied Sciences*, vol. 9, no. 24, Article ID 5534, 2019.

[22] R. Perera, D. Tarazona, A. Ruiz, and A. Martín, "Application of artificial intelligence techniques to predict the performance of RC beams shear strengthened with NSM FRP rods. Formulation of design equations," *Composites Part B: Engineering*, vol. 66, pp. 162–173, 2014.

[23] M. Shariati, M. S. Mafipour, J. H. Haido et al., "Identification of the most influencing parameters on the properties of corroded concrete beams using an adaptive neuro-fuzzy inference system (ANFIS)," *Steel & Composite Structures*, vol. 34, no. 1, pp. 155–170, 2020.

[24] A. Karimipour, J. Mohebbi Najm Abad, and N. Fasihihour, "Predicting the load-carrying capacity of GFRP-reinforced concrete columns using ANN and evolutionary strategy," *Composite Structures*, vol. 275, Article ID 114470, 2021.

[25] J. H. Haido, "Prediction of the shear strength of RC beam–column joints using new ANN formulations," *Structures*, vol. 38, pp. 1191–1209, 2022.

[26] L. Chen, P. Fakharian, D. Rezazadeh Eidgahee, M. Haji, A. Mohammad Alizadeh Arab, and Y. Nouri, "Axial compressive strength predictive models for recycled aggregate concrete filled circular steel tube columns using ANN, GEP, and MLR," *Journal of Building Engineering*, vol. 77, Article ID 107439, 2023.

[27] V. K. Ojha, A. Abraham, and V. Snášel, "Metaheuristic design of feedforward neural networks: a review of two decades of research," *Engineering Applications of Artificial Intelligence*, vol. 60, pp. 97–116, 2017.

[28] X.-S. Yang, "Review of metaheuristics and generalized evolutionary walk algorithm," arXiv preprint arXiv, 2011.

[29] J. Li, G. Yan, L. H. Abbud et al., "Predicting the shear strength of concrete beam through ANFIS-GA–PSO hybrid modeling," *Advances in Engineering Software*, vol. 181, Article ID 103475, 2023.

[30] I. Faridmehr, M. L. Nehdi, and M. Hajmohammadian Baghban, "Novel informational bat-ANN model for predicting punching shear of RC flat slabs without shear reinforcement," *Engineering Structures*, vol. 256, Article ID 114030, 2022.

[31] N. Concha, J. R. Aratan, E. M. Derigay, J. M. Martin, and R. E. Taneo, "A hybrid neuro-swarm model for shear strength of steel fiber reinforced concrete deep beams," *Journal of Building Engineering*, vol. 76, Article ID 107340, 2023.

[32] M. Imran Waris, V. Plevris, J. Mir, N. Chairman, and A. Ahmad, "An alternative approach for measuring the mechanical properties of hybrid concrete through image processing and machine learning," *Construction and Building Materials*, vol. 328, Article ID 126899, 2022.

[33] M. I. Waris, J. Mir, V. Plevris, and A. Ahmad, "Predicting compressive strength of CRM samples using Image processing and ANN," *IOP Conference Series: Materials Science and Engineering*, vol. 899, no. 1, Article ID 012014, 2020.

[34] M. S. Sandeep, K. Tiprak, S. Kaewunruen, P. Pheinsusom, and W. Pansuk, "Shear strength prediction of reinforced concrete beams using machine learning," *Structures*, vol. 47, pp. 1196–1211, 2023.

[35] A. Ahmad, Q. Z. Khan, and A. Raza, "Reliability analysis of strength models for CFRP-confined concrete cylinders," *Composite Structures*, vol. 244, Article ID 112312, 2020.

[36] G. M. Kotsovou, A. Ahmad, D. M. Cotsovos, and N. D. Lagaros, "Reappraisal of methods for calculating flexural capacity of reinforced concrete members," *Proceedings of the Institution of Civil Engineers—Structures and Buildings*, vol. 173, no. 4, pp. 279–290, 2020.

[37] A. Raza, Q. Z. Khan, and A. Ahmad, "Prediction of axial compressive strength for FRP-confined concrete compression members," *KSCE Journal of Civil Engineering*, vol. 24, no. 7, pp. 2099–2109, 2020.

[38] M. D. Kotsovos, *Compressive-Force Path Method: Unified Ultimate Limit-State Design of Concrete Strctures*, Engineering Materials (ENG.MAT.), Springer, 2014.

[39] P. Code, *Eurocode 2: Design of Concrete Structures-Part 1-1: General Rules and Rules for Buildings*, British Standard Institution, London, 2005.

[40] A. ACI, *Building Code Requirements for Structural Concrete and Commentary*, American Concrete Institute, 2014.

[41] J. G. Wood, "Pipers row car park, wolverhampton," Quantitative Study of the Causes of the Partial Collapse on 20th March, 1997.

[42] A. Ahmad, N. D. Lagaros, and D. M. Cotsovos, "Neural network-based prediction: the case of reinforced concrete members under simple and complex loading," *Applied Sciences*, vol. 11, no. 11, Article ID 4975, 2021.

[43] I. A. Basheer and M. Hajmeer, "Artificial neural networks: fundamentals, computing, design, and application," *Journal of Microbiological Methods*, vol. 43, no. 1, pp. 3–31, 2000.

[44] R. Poli, J. Kennedy, and T. Blackwell, "Particle swarm optimization," *Swarm Intelligence*, vol. 1, no. 1, pp. 33–57, 2007.

[45] K. Premalatha and A. M. Natarajan, "Hybrid PSO and GA for global maximization," *International Journal of Open Problems in Computer Science and Mathematics*, vol. 2, no. 4, pp. 597–608, 2009.

[46] F. Marini and B. Walczak, "Particle swarm optimization (PSO): A tutorial," *Chemometrics and Intelligent Laboratory Systems*, vol. 149, pp. 153–165, 2015.

[47] A. J. Nebro, J. J. Durillo, J. Garcia-Nieto, C. C. Coello, F. Luna, and E. Alba, "SMPSO: a new PSO-based metaheuristic for multi-objective optimization," in *2009 IEEE Symposium on Computational Intelligence in Multi-Criteria Decision-Making (MCDM)*, pp. 66–73, IEEE, Nashville, TN, USA, March 2009.

[48] X.-S. Yang, "A new metaheuristic bat-inspired algorithm," in *Nature inspired cooperative strategies for optimization (NICSO 2010)*, J. R. González, D. A. Pelta, C. Cruz, G. Terrazas, and N. Krasnogor, Eds., vol. 284 of *Studies in Computational Intelligence*, pp. 65–74, Springer, Berlin, Heidelberg, 2010.

[49] X.-S. Yang and A. Hossein Gandomi, "Bat algorithm: a novel approach for global engineering optimization," *Engineering Computations*, vol. 29, no. 5, pp. 464–483, 2012.

[50] I. Fister Jr., D. Fister, and X.-S. Yang, "A hybrid bat algorithm," arXiv preprint arXiv, 2013.

[51] A. Ahmad and D. M. Cotsovos, "Reliability analysis of models for predicting T-beam response at ultimate limit response," *Proceedings of the Institution of Civil Engineers—Structures and Buildings*, vol. 176, no. 1, pp. 28–50, 2023.

[52] G.-D. Wu and S.-L. Lo, "Effects of data normalization and inherent-factor on decision of optimal coagulant dosage in water treatment by artificial neural network," *Expert Systems with Applications*, vol. 37, no. 7, pp. 4974–4983, 2010.

[53] A. Azadeh, M. Saberi, and M. Anvari, "An integrated artificial neural network fuzzy C-means-normalization algorithm for performance assessment of decision-making units: the cases of auto industry and power plant," *Computers & Industrial Engineering*, vol. 60, no. 2, pp. 328–340, 2011.

[54] T. Zhang and X. You, "Improvement of the training and normalization method of artificial neural network in the prediction of indoor environment," *Procedia Engineering*, vol. 121, pp. 1245–1251, 2015.

[55] D. Bompa and T. Onet, "Punching shear strength of RC flat slabs at interior connections to columns," *Magazine of Concrete Research*, vol. 68, no. 1, pp. 24–42, 2016.

[56] M. H. Abdallah, Z. A. Thoeny, S. N. Henedy et al., "The machine-learning-based prediction of the punching shear capacity of reinforced concrete flat slabs: an advanced M5P model tree approach," *Applied Sciences*, vol. 13, no. 14, Article ID 8325, 2023.

[57] S. Liang, Y. Shen, and X. Ren, "Comparative study of influential factors for punching shear resistance/failure of RC slab–column joints using machine-learning models," *Structures*, vol. 45, pp. 1333–1349, 2022.

[58] M. Lapi, H. Fernandes, M. Orlando, A. Ramos, and V. Lúcio, "Performance assessment of flat slabs strengthened with a bonded reinforced-concrete overlay," *Magazine of Concrete Research*, vol. 70, no. 9, pp. 433–451, 2018.

[59] H. Salem, H. Issa, H. Gheith, and A. Farahat, "Punching shear strength of reinforced concrete flat slabs subjected to fire on

their tension sides," *HBRC Journal*, vol. 8, no. 1, pp. 36–46, 2019.

[60] M. M. G. Inácio, M. Lapi, and A. Pinho Ramos, "Punching of reinforced concrete flat slabs–rational use of high strength concrete," *Engineering Structures*, vol. 206, Article ID 110194, 2020.

[61] Y. David, "Punching strength of reinforced concrete slabs," *Journal Proceedings*, vol. 63, no. 5, pp. 527–542, 1966.

[62] H. Marzouk and A. Hussein, "Experimental investigation on the behavior of high-strength concrete slabs," *Structural Journal*, vol. 88, no. 6, pp. 701–713, 1992.

[63] Y. Shen, L. Wu, and S. Liang, "Explainable machine learning-based model for failure mode identification of RC flat slabs without transverse reinforcement," *Engineering Failure Analysis*, vol. 141, Article ID 106647, 2022.

[64] H.-T. Hu and W. C. Schnobrich, "Nonlinear analysis of cracked reinforced concrete," *Structural Journal*, vol. 87, no. 2, pp. 199–207, 1990.

[65] A. Ahmad, M. U. Arshid, T. Mahmood, N. Ahmad, A. Waheed, and S. S. Safdar, "Knowledge-based prediction of load-carrying capacity of RC flat slab through neural network and FEM," *Mathematical Problems in Engineering*, vol. 2021, Article ID 4528945, 18 pages, 2021.

[66] M. D. Kotsovos, *Compressive Force-Path Method*, Springer, Cham Heidelberg New York Dordrecht London, 2014.

[67] A. Pérez Caldentey, P. Padilla Lavaselli, H. Corres Peiretti, and F. Ariñez Fernández, "Influence of stirrup detailing on punching shear strength of flat slabs," *Engineering Structures*, vol. 49, pp. 855–865, 2013.